



**2019 SpaceX Hyperloop Pod Competition Final  
Design Package**



**2018 - 2019**



Revised on 9th January, 2019

Prepared by the uWinLoop Hyperloop Team.

Prepared for Space Exploration Technologies Corp. for the Hyperloop Pod Competition.

© 2019 by uWinLoop.

All rights reserved. Not for public distribution. Yet.

Document approved for submission by the uWinLoop executive team on January 10, 2019.

1. Introduction	7
1.1. Team History	7
1.2. Member List	8
1.3. Acknowledgements	9
2. Top-level design	9
2.1. Summary of Pod Design	10
2.2. Weight by Pod Subsystems	10
3. Loading and Unloading Plan	11
3.1. Pod Moving Procedure to Staging Area	12
3.2. Ready-to-Launch Procedure	12
3.3. Ready-to-Remove Procedure	12
3.4. Pod Moving Procedure from Staging Area	13
4. Scalability	13
4.1. System Size	13
4.2. Maintenance	15
4.2.1. Track	15
4.2.2. Pod	15
5. Propulsion	16
5.1. Overview	16
	17
5.2. Structural Design	18
5.3. LIM Performance	19
5.4. Thermal Analysis	27
5.5. Test and Validation	29
5.6. FMEA	30
6. Braking	36
6.1. System Overview	36
6.2. Friction Braking	36
6.2.1. Operation and Performance of Friction Braking	37
6.2.2. Thermal Analysis and Material Selection for Friction Braking	44
6.2.3. Testing and Validation	46
6.2.4. FMEA	47

6.3.	LIM Braking	47
6.3.1.	Performance of LIM Braking	47
6.3.2.	Thermal Analysis for LIM Braking	48
6.3.3.	Testing and Validation	48
6.3.4.	FMEA	49
7.	Stabilizers	50
7.1.	Overview	50
7.2.	LCM	50
7.2.1.	Structural Design	51
7.2.2.	Stress analysis	51
7.2.3.	Test and Validation	51
7.3.	VCM	52
7.3.1.	Structural Design	52
7.3.2.	Stress Analysis	53
7.3.3.	Tests & Validation	54
8.	Structural	55
8.1.	Overview	55
8.2.	Shell	56
8.2.1.	Overview	56
8.2.2.	Structural Design	56
8.2.3.	CFD Analysis	57
8.2.4.	Testing and Validation	58
8.3.	Frame	58
8.3.1.	Structural Design Cases	58
8.3.1.1.	Initial Acceleration Case	59
8.3.1.2.	Nominal Deceleration	59
8.3.1.3.	Reasonably Foreseeable Off-Nominal Crash	60
8.3.1.4.	Thermal Analysis	60
8.3.1.5.	Testing and Validation	60
9.	Power	61
9.1.	Overview	61
9.2.	Battery	62
9.2.1.	Design	62

9.2.1.1.	High Voltage Battery Pack	62
9.2.2.	(25.9)V DC battery	66
9.2.3.	Battery safety:	67
9.3.	BMS	68
9.3.1.	Design	68
9.3.2.	SOC	68
9.3.3.	Cell balancing	68
9.3.4.	Controls BMS	68
9.4.	Inverter	69
9.4.1.	Overview	69
9.4.2.	Design	69
9.4.2.1.	Gate Driver	69
9.4.2.2.	Switches (IGBT)	70
9.4.2.3.	Microcontroller	71
9.4.2.4.	Safety	71
9.5.	Failsafes	71
9.5.1.	Battery	71
9.6.	Pressure Vessel	71
9.6.1.	Pressure Vessel for High Voltage Battery	71
9.6.2.	Pressure Vessel for Control Battery and Controls	72
9.6.3.	Safety features	73
9.6.4.	Pressure Vessel FEA Analysis	73
9.7.	Testing	75
9.7.1.	Battery	75
9.7.1.1.	Battery Cell Testing:	75
9.7.1.2.	Battery Pack Testing:	75
9.7.1.3.	Pressure leakage testing	75
9.7.2.	BMS	76
9.7.3.	Inverter	76
9.8.	Failure Modes	78
10.	Embedded	79
10.1.	Introduction	79
10.2.	Main Embedded Board (MEB)	79

10.3.	Sensor Hubs	80
10.4.	Control Hub	81
10.5.	BMS Hub	81
10.6.	Testing	81
10.6.1.	Vacuum testing	81
10.6.2.	Hardware in loop	81
10.7.	Single Point of Failure	82
10.8.	Failure Modes	82
10.9.	Embedded Bill of Materials	82
11.	Control systems	84
11.1.	Overview	84
11.2.	Pod state diagram	84
11.3.	Heartbeat	85
11.4.	Communication System	85
11.5.	Navigation System	85
11.6.	Failure Modes	85
12.	Next steps	87
12.1.	Design Phase	87
12.2.	Test Phase	87
13.	Pod Production Schedule	88
		88
14.	Bill of Materials	89
15.	Financing	89
16.	References	90

## 1. Introduction

### 1.1. Team History

Founded in October of 2017 uWinLoop is a team of 22 students from the University of Windsor and St. Claire College. Primarily an undergraduate team, uWinLoop is composed of students from mechanical, electrical, and industrial engineering, as well as students from computer science.

During the 2018 competition season, uWinLoop had a contributing partnership with the University of Waterloo's Hyperloop team, Waterloo. The partnership greatly benefitted both teams, creating a chance for undergraduate students to collaborate, share ideas, and create original work. Undergraduate students at uWinLoop also developed a deeper understanding of the requirements of the SpaceX Hyperloop Pod Competition.

Unfortunately, for the 2018 competition season at SpaceX, uWinLoop was eliminated in the preliminary design briefing stage, promptly ending our partnership with Waterloo as well. However, for the 2019 competition season, University of Windsor students have been motivated and determined to take uWinLoop to the final competitions; volunteering much time and effort, undergraduate and masters students are ready to bring the uWinLoop Pod to life.

During the last year, uWinLoop has continually and independently developed concepts and models needed for a successful application into the SpaceX Hyperloop Pod Competition. UWinLoop feels that this direction of technical development is the future of safe, sustainable, reliable hyperloop technology to encourage future societal growth and development.

## 1.2. Member List

Structure: Faculty, team leadership, team members by sub-team/focus

**President**  
Stefan Sing

### Team Leads

<b>Mechanical</b>	<b>Electrical</b>	<b>Software/Controls</b>
Don Algama	Leonard Hui	Kevin Shi
<b>Braking</b>	<b>Linear Induction Motor</b>	<b>Administrative Lead</b>
Matthew Marcoccia	Michael Thamm	Stefan Sing

### Team Members (Mechanical)

<b>Stabilizers</b>	<b>Frame</b>	<b>Shell</b>
Alex Xu	Kiran Kothandaraman	Patrick Perron
Srikar Kadavakuti	Alex Xu	
Nikunj Patel		
Kiran Kothandaraman		
Weiling Zhou		
<b>Braking</b>		<b>Pressure Vessel</b>
Matthew Marcoccia		Dhairya Dhamija
Nikhil Akbari		Nikhil Akbari
Dhairya Dhamija		
Nikunj Patel		

**Integration Leads:** Matthew Marcoccia

### Team Members (Electrical)

<b>Linear Induction Motor</b>	<b>Power</b>
Michael Thamm	Tochukwu Ibegbulam
	Pancham Thaker
	Vivek Punjabi
	Leonard Hui
<b>Administrative Members</b>	<b>CAD Design</b>
Bart Hoxha	Mohammed Alsalah
Brian Luong	Luka Mlinarevic
	Kiran Kothandaraman

### 1.3. Acknowledgements

uWinLoop would like to extend its gratitude and appreciation to the University of Windsor Dean of Engineering, Dr. Mehrdad Saif, as well as Dr. Rashid Rashidzadeh, Dr. Alexandr Cherniaev, Dr. Narayan Kar, Ivan Canjar, Domenico Rossi and all the technologists, administrative and support staff at the Faculty of Engineering at the University of Windsor. Your continued support and guidance is sincerely appreciated.

The admin team would like to sincerely thank all of the team members for their efforts, especially down the final stretch. We were able to accomplish what other schools have with ten time the members. This is something we should be very proud of, excellent work uwinLoop!

## 2. Top-level design

## 2.1. Summary of Pod Design

Aiming to compete in the 2019 competition, uWinLoop was intent on breaking the current record of 457km/h. To achieve this, the pod must collectively be lightweight, capable of direction along the track, and capable of accelerating and decelerating in a controlled manner. These limitations inspired a pod which weighs 273kg.

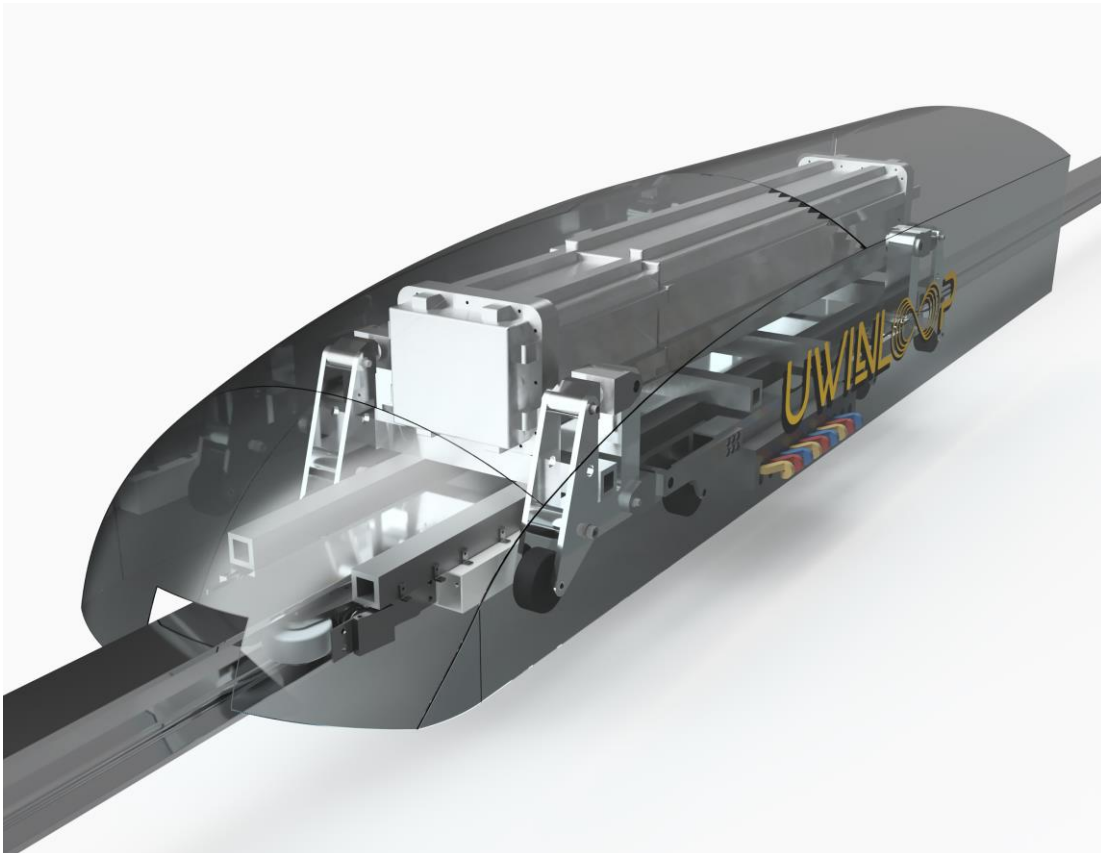


Figure 1, Overall Pod

## 2.2. Weight by Pod Subsystems

The pod is a synthesis of six sub-systems: Propulsion, Brakes, Stabilizers, Structural, Power, Embedded and Control Systems. Below is a table showing the masses of each sub-system.

Sub System	Mass (kg)
Propulsion	69
Braking	52

Stabilizers	20
Structural	37
Electrical	35
Pressure Vessels	60

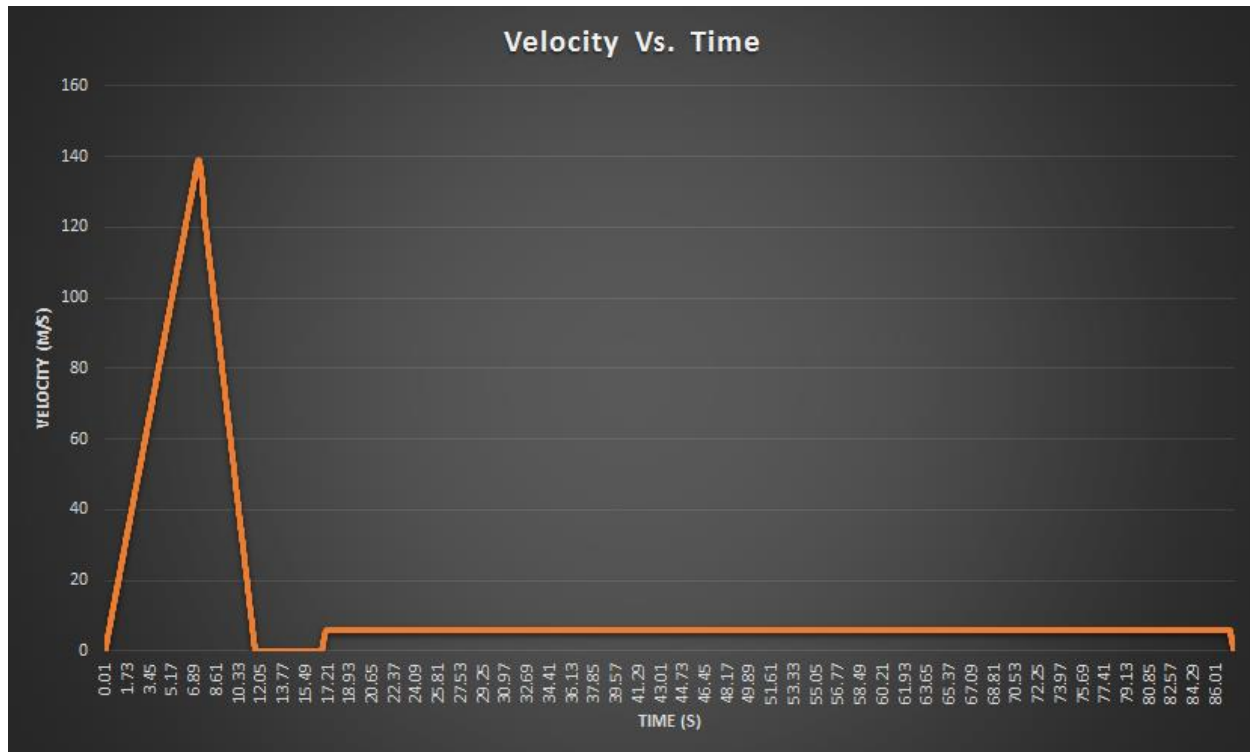


Figure 2, Pod Velocity Profile

### 3. Loading and Unloading Plan

Once the pod arrives at Hawthorne, California. A folding workshop crane and wood pallet will be used to move the pod to designated locations.

### 3.1. Pod Moving Procedure to Staging Area

Due to the weight of the pod being 273kg, a forklift with web slings will be used to move the pod. The following outlines the procedure that would be implemented in the staging area:

1. Pod will be turned off with all actuation systems set to manual retract position.
2. The shell will be removed exposing the swivel hoist rings
3. Weblings slings will be attached to these swivel hoist rings and the forklift swivel hook adapter
4. Pod will be lifted onto the Loading Platform
5. Web slings will then be detached from the pod and forklift
6. Team will roll pod onto the alignment rail where the front wheels of the LCM will be making first contact with the I-beam.
7. Pod will now be switched on and the shell will be re-attached
8. Tube doors will be closed and pod will initiate the Ready-to-Launch Procedure which is described below

### 3.2. Ready-to-Launch Procedure

Once the pod is in the tube and has been depressurized, the pod would undergo the Ready-to-Launch procedure.

1. Check all heart beats are being received
2. Check if network telemetry is being received
3. Verify that motion encoder is reading zero
4. Verify value from barometric sensors corresponds to predicted value
5. Verify values from proximity sensors corresponds to predicted value
6. Brakes are disengaged
7. Verify proximity sensors validate that brakes are disengaged
8. Check voltage and current readings of LIM unit corresponds to predicted value

### 3.3. Ready-to-Remove Procedure

After the pod has come to a complete stop it and the tunnel had been re-pressurized the pod will perform the Ready to Remove procedure as listed below

1. Verify value from barometric sensors corresponds to predicted value
2. Open Pressure release valves
3. Check that HV battery is in safe mode
4. Check that brakes are disengaged
5. Apply manual locks to brakes to keep them retracted.

### 3.4. Pod Moving Procedure from Staging Area

Post-performance, pod components would be extremely hot and pose a health and safety hazard (for example, serious burns). Therefore, a limited number of individuals will be handling this stage of transport.

This process will include:

1. Disengage brakes, mechanically lock it in there retracted position and turn off the pod
2. Once the tunnel doors are open, roll the pod to the Exit Area
3. Remove the shell and attach the slings onto the swivel hoist rings and the forklift swivel hook adapter
4. Place the pod onto the wooden pallet and remove the sling attachment on the forklift swivel hook adapter to the folding workshop crane

## 4. Scalability

### 4.1. System Size

LIM - Linear induction motors must increase in size to propel a much larger pod. Furthermore, to propel the full scale pod, several aspects of the LIM must respectively increase, including: the number of wires, length of the windings, number of windings, and size of the stator. The size of each SLIM will grow by a factor of 6-8 if the pod were to maintain only two SLIMs. Accompanying the increase in pod size is an increase in space; the number of SLIMSs can be increased from more than just two. Multiple SLIM units can be used in the pod to not only increase thrust, but to also evenly distribute the thrust forces being generated along the body of pod. The amount of power from a series of much larger LIMs should propel the pod at close to supersonic speeds.

Power Supply - Power supply for the LIMs will increase with respect to the increase in LIM size. The estimated power draw for Linear Induction Motors of this scale would be in the order of 2-3MW. This value is based on linear scaling of the future LIM design for the quarter scale pod design. Power supply for the SLIMs can be distributed in the same fashion as our current power supply/battery management system. This might require the use of superconductors in order to minimize the weight of the pod.

Braking - Braking capabilities must also account for the increase in LIM size; the LIM will be used for partial braking of the system. Thrust capabilities will be proportional to the braking capabilities. The friction braking system could be scaled up to a similar level to that of freight trains. A braking system of this size would likely be powered by hydraulics. Limitations of this system would depend on the materials of the center rails/tracks and the brake pads. To minimize braking distance, a cooling system must be implemented along with an EC braking system. This can easily be done by actuating large banks of permanent magnets closer or further away from the tracks/beams. The actuators needed for the EC module must be just

strong enough to overcome the force of friction. Therefore, an EC braking system can easily be implemented into the design.

Stabilizers - Depend heavily on the infrastructure of the guides/rails in which the pod is riding along. Assuming the same method as the pod competition, stabilizers would easily be scalable in terms of damping. Adding more to overcome the larger forces is also possible as they are relatively small in size. An issue that may come up is the speed of the pod: the stabilizers will have to rotate at very high speeds, and the bearings supporting the wheels will have to be able to support such high speeds. This can be fixed by greatly increasing the diameter of the stabilizing wheels.

Frame - The full scale pod would have a frame design that would require it to support the load forces of all the subsystems in the pod and at the same time provide a structure that would be able to withstand sudden decompression of the tube in an emergency. This would result in a similar structure to what is currently being used in fuselages for passenger planes but more structured as the exterior environment of the pod would be of very low pressure. The frame would still have to be designed light without compromising safety.

Shell - Shell would have to be designed with the same criteria as the frame. However, significant aerodynamic properties need to be considered as the projection area is now larger and the increased length of the pod would increase the turbulent boundary layer. Wake generated due to high speed (supersonic) will significantly affect the design criteria of the shell of the pod and as we achieve the supersonic speed mass around the pod will move at sonic speed (Kantrowitz limit) thus shell design needs to account for the mass that is collected in front of the pod based on aerodynamic shape or to include compressor on board. Stream wise stability of the pod affects the comfort of the passengers as well as structural integrity of the pod.

Controls - Controls will remain fairly similar for the overall operation of the pod. The same level of fail safes and safety procedures will be followed when controlling propulsion, braking, cooling, power supply and stabilizers. There will, however, be a new sub-level of controls that will directly relate to the transportation of passengers. These are mainly safety controls that are not directly related to the operation of the pod, but rather the safety and comfort of passengers. The logic used to control the small pod would effectively be used to control a full scale pod.

Cooling - Currently, pod cooling systems have not been implemented; however, they are being developed for future versions of the LIM (as well as braking systems). This is what is used for this portion of the report. The LIM cooling system will most likely be a combination of large heat sinks and a thermofluid closed loop system. This can be scaled to a larger model by simply increasing the size of the sinks and/or the size of the hydraulic pump to move the thermofluid through the closed vein system. A more practical solution is to add a compressor/evaporator cycle to this fluid system; for example, rather than having the fluid simply transfer heat into a sink, a refrigeration cycle can be utilized to expel heat out of the pod. This could be used to cool all of the subsystems if designed properly.

## 4.2. Maintenance

### 4.2.1. Track

Periodic maintenance would be required of the track to ensure continuous operation of the system and avoid accident. Following are the inspection and maintenance that needs for continuous uninterrupted operation:

- 1) Check for alignment of track section.
- 2) Possible debris gathered on the track
- 3) Corrosion and crack propagation

### 4.2.2. Pod

Pod maintenance is of great essence as safety of the passengers are at stake if it fails while in operation or is inside the vacuum tube. Following is the sets of technical maintenance that would require to ensure continuous operation.

- 1) LIM
  - a) Cable connections
  - b) Controls and sensors
  - c) battery/power connection
  - d) Wire conditions
- 2) Brake
  - a) Friction Pad material wear
  - b) Actuator operation
  - c) Controls and sensor to avoid undesirable situation
  - d) Casing cleanup of the brake
- 3) Pressure vessel
  - a) Check all check Valves
  - b) Ensure all parts (connectors) are sealed and leak proof
  - c) Barometer sensor operation is crucial to ensure the safety of the passengers on board
  - d) Controls operation and ability to control various pressure relief valve in case of emergency should be checked at timely interval.
- 4) Battery
  - a) Cell Voltage check
  - b) Battery pack voltage check
  - c) Electrical connections
- 5) Structural (Frame and Stabilizers)
  - a) Structural Integrity
  - b) Proper lubrication
  - c) Joint conditions
- 6) Cooling System
  - a) Coolant level
  - b) System pressure

## 5. Propulsion

### 5.1. Overview

To determine the most suitable propulsion system for our pod, instigations were made into many variations of inductive propulsion. This was due to the high friction losses created at high speeds for friction drives. These types of system have already been rigorously tested and perfected which leaves little room for improvement from our team.

This prompted further investigation of linear motors. The initial focus was on linear induction motors (LIM). As indicated in the name, these types of motors use the principle of induction created from AC current flowing through the primary of the motor to induce eddy currents in the secondary. This will create a repulsive force between the two magnetic fields produced by the primary and secondary. Another variation of this is the synchronous linear motor, which has similar fundamentals, but differs only in the secondary. This difference is that the secondary plate is composed of permanent magnets used to create a magnetic field.

Since the provided SpaceX track creates specific constraints in term of the secondary material and configuration, the choice of which linear motor to pursue must be carefully considered. Evidently, a permanent magnet secondary is not an option since the sub-track and I-beam are made of aluminum and are provided by SpaceX.

A double-sided linear induction motor (DLIM) around the I-beam was first conceptualized, which would have provided excellent lateral stability and appropriate thrust force. The reason this concept was not chosen was due to the constrained space on the I-beam provided by SpaceX. This creates low flexibility and room for error.

Finally, the decision was made to test a single-sided linear induction motor on each sub-track since there was plenty of room to work with, and the width of sub-track was large enough to create a wide variety of SLIM concepts. Additionally, the output results for thrust and levitation force would be doubled since two SLIMs would be used. Room for error exists in the provided sub-track design. There is no back iron behind the aluminum plate, cutting the magnetic flux flow. Additionally, the constrained sub-track thickness constrains the SLIM size since increasing the power rating of SLIM drastically will cause saturation in the secondary. This must be carefully considered.

The simulations and plotted results in the propulsion section were all made using the CAD software, ANSYS Electronics Desktop. 3D Maxwell designs were made to simulate the SLIM designs which were modeled in a transient magnetic environment. This allows for time varying fields and plots to be realized, which is very important to this competition and the characterization of the SLIM.

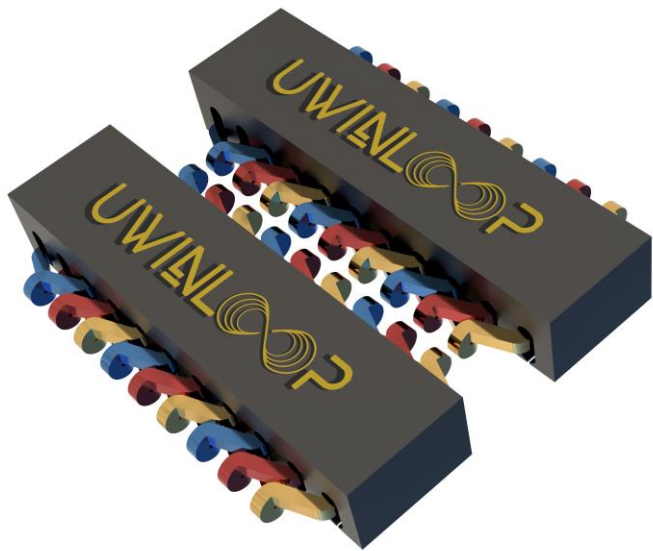


Figure 3, CAD of LIMs

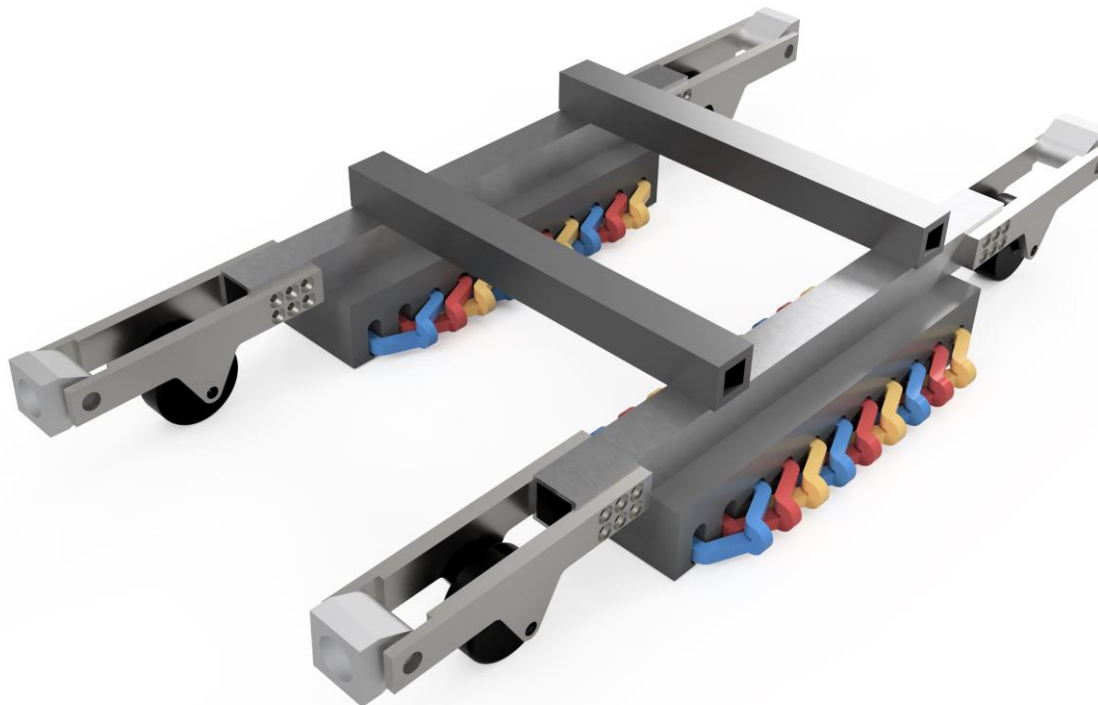


Figure 4, CAD of LIM Inside Frame

## 5.2. Structural Design

### Circuit diagram

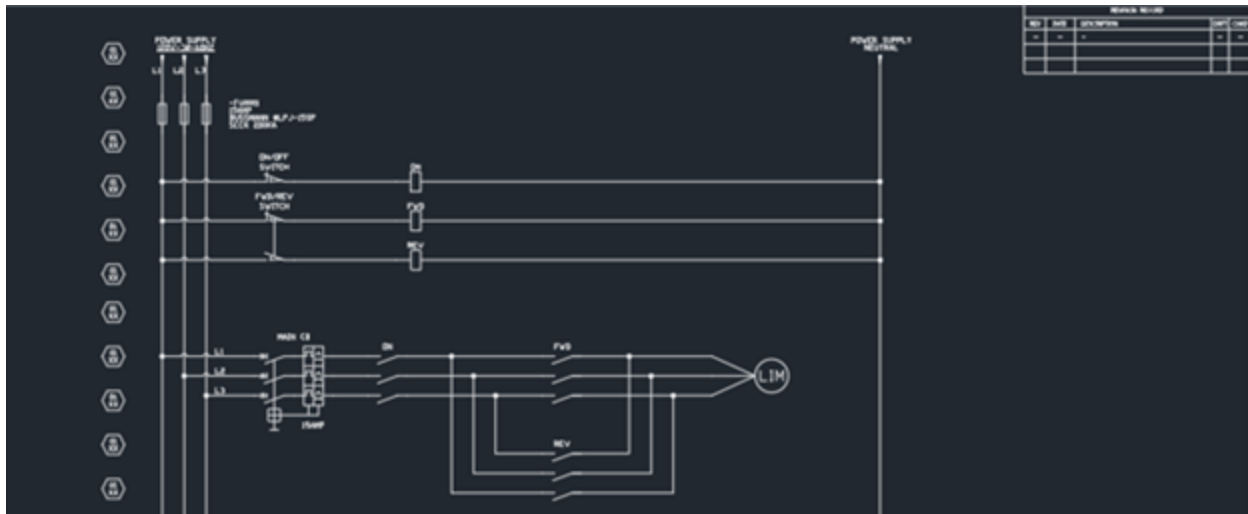


Figure 5, Onboard Control Circuit for SLIM

This circuit was designed to make sure that the SLIM will never receive more power than it was designed for. The 3 phase input lines coming directly from the battery are individually fused. Below this fusing are 3 contactors. 2 of these contactors are dedicated to the switching of SLIM thrust direction. This can be seen in the contactor wires which are labelled FWD and REV and these can freely open and close, given the contactor state. It is important to note that the switch before the FWD and REV contactors there is a linked switch that allows only 1 of these contactors to be hot at once. This prevents the current to choose the path of least resistance, which will always be FWD. This would be a major issue in terms of using SLIM for breaking. The remaining contactor is used as an ON/OFF control. This contactor is labelled ON and can be seen controlling the 3 phases above the SLIM and the FWD and REV contacts. Lastly, there is a 3 phase circuit breaker above all of these connections to ensure that the SLIM will never be supplied with a larger power than it is rated for.

To determine the circuit breaker sizing, the max allowable current input for SLIM was assessed. This can be determined by the max allowable current in transmission wiring for the AWG size chosen for the SLIM windings in Table 1. For example, design 1 was chosen to have a wire gauge of 14, which has a tolerance of 5.9A for transmission wiring. Therefore the circuit breaker will be sized to this max value so the wires will not be permanently damaged during operation. Since this table is purely an approximation for transmission wiring sizing, further testing must be conducted in a practical setting to ensure that the proper sizing is chosen.

2/26/2018 American Wire Gauge Table (AWG): Brown and Sharpe [JPG format]

AWG wire size (solid)	Area (CM) Squared Mil	Resistance per 1000 ft (In Ohms and 20 degree)	Diameter (inches)	Maximum current for Chassis Wiring (Amp)	Maximum Current for Transmission
0000	211600	0.049	0.46	380	302
000	167810	0.0618	0.40965	328	239
00	133080	0.078	0.3648	283	190
0	105530	0.0983	0.32485	245	150
1	83694	0.124	0.2893	211	119
2	66373	0.1563	0.25763	181	94
3	52634	0.197	0.22942	158	75
4	41742	0.2485	0.20431	135	60
5	33102	0.3133	0.18194	118	47
6	26250	0.3951	0.16202	101	37
7	20816	0.4982	0.14428	89	30
8	16509	0.6282	0.12849	73	24
9	13094	0.7921	0.11443	64	19
10	10381	0.9989	0.10189	55	15
11	8234	1.26	0.09074	47	12
12	6529	1.588	0.0808	41	9.3
13	5178.4	2.003	0.07196	35	7.4
14	4106.8	2.525	0.06408	32	5.9
15	3256.7	3.184	0.05707	28	4.7

Table 1: AWG table for SLIM design

### 5.3. LIM Performance

#### High level explanation of each component

- Include wiring diagrams, Sims, CAD models

Table 2: Iterations of SLIM Design

Parameters	Design 1	Design 2
Line Voltage (Vac)	400	400
Power Required (kW)	2.15	6.46
Number of Phases	3	3
Frequency (Hz)	60	60
Air Gap (mm)	5.08	2.54
Slip	0.1	0.2
Rotor Velocity (m/s)	8	16.3
Poles	3	3
Turns Per Slot	100	55
Slots	11	

Wire Gauge	14	10
Stator Length (m)	0.508	0.508
Stator Width (m)	0.254	0.254
Slot Height (cm)	4.699	4.699
Slot Width (cm)	1.905	1.905
Yoke Height (cm)	3.302	3.302
Slot Pitch (cm)	4.445	4.445
Coil Pitch	2	2
Coil Span (electrical degrees)	120	120

From table 2 it is shown that a slip of 0.1 was used for the SLIM design. The reasoning behind this slip value comes from the characteristics of SLIM normal force. This value is composed of a repulsive and attractive component governed by the equation:

$$F_{yy} = \frac{1}{l\lambda\mu_0} \left[ \frac{\bar{V}}{v_{sy}Z_m} \right]^2 \frac{1 - (R_mS)^2}{(\cosh \beta g)^2 + (R_mS \sinh \beta g)^2}$$

It is observed and proven theoretically that the attractive component of normal force is at a maximum when the motor runs at synchronous speed, resulting in a slip of 0. The opposite can be observed when the slip is approximately equal to 1. Another way to realize this is that the force becomes increasingly repulsive as the rotor speed increases or as the operating range tends to a higher frequency supply.

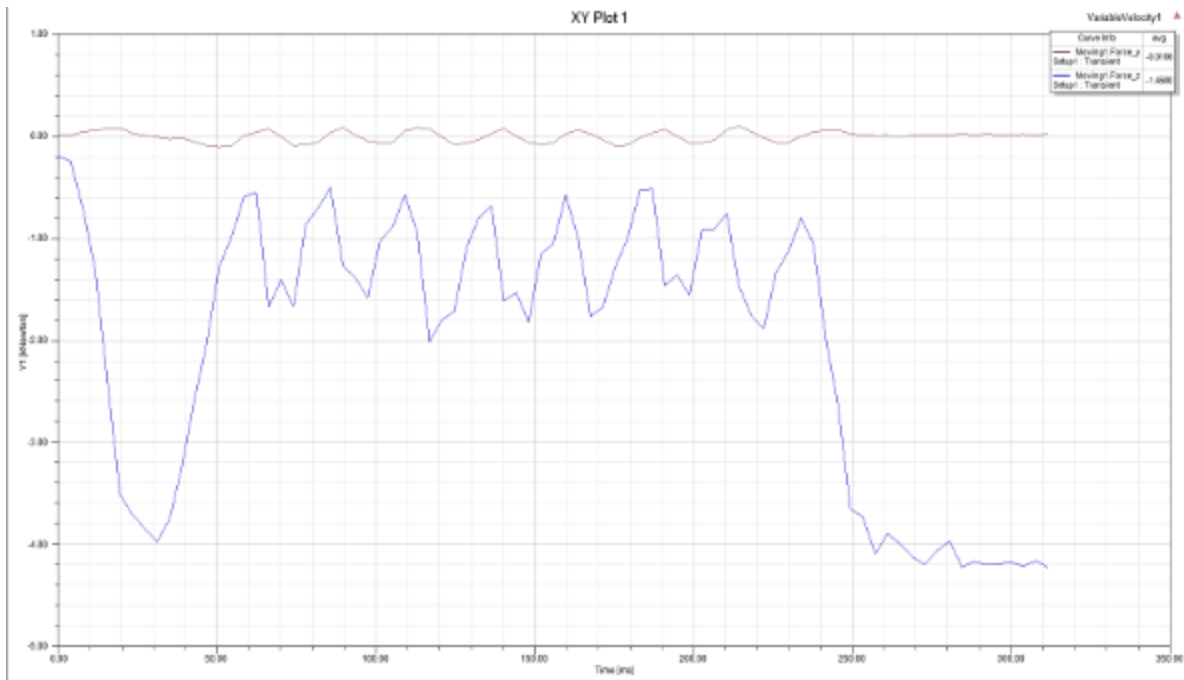


Figure 6: Levitation and Thrust Force vs. Time for Design 2

A good representation of this concept is observed in the results of figure 6. This shows that the force in the range of 0-240ms is much less attractive than in the range of 240-310ms. This is because the rotor velocity plot corresponding to this plot remains constant until 240ms before dropping to 0.

This concept must further be analyzed, since choosing a very high slip doesn't result in good performance. To accommodate this, the slip must be chosen at a value where the normal force is mainly repulsive and the slip is not high enough to create an unrealistic amount of power loss. As a result, the slip value of 0.1 was chosen for SLIM design. Further iterations will be made to optimize this using swept variables in the ANSYS Electronic simulations.

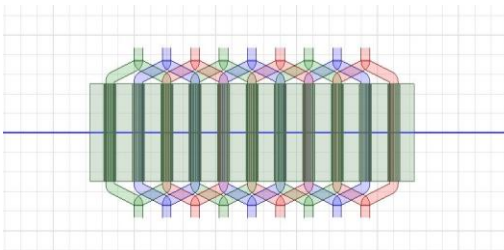


Figure 7: Top View of Finalized SLIM Design

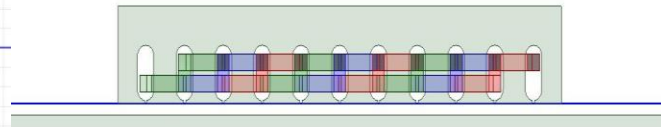
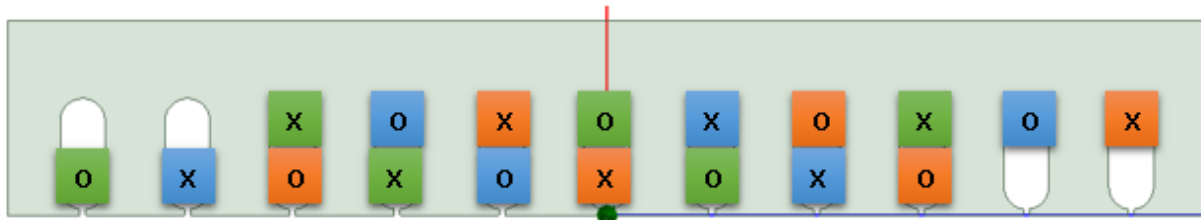


Figure 8: Side View of Finalized SLIM



**Red = Phase A, Blue = Phase B, Green = Phase C. X = Wire into page, O = Wire out of page.**

Figure 9: Winding Design Layout for SLIM design

The SLIM is designed in a 2 layer configuration with 3 phase coil windings. This can be seen in figure 9. Additionally, this design has 3 poles and each neighboring winding has opposite current direction to create varying magnetic polarity. The reasoning behind a double layer, fractional pitch winding configuration is its ability to mitigate harmonics in the voltage wave. To further characterize the SLIM, a slot/pole/phase ratio is determined to be 11/9.

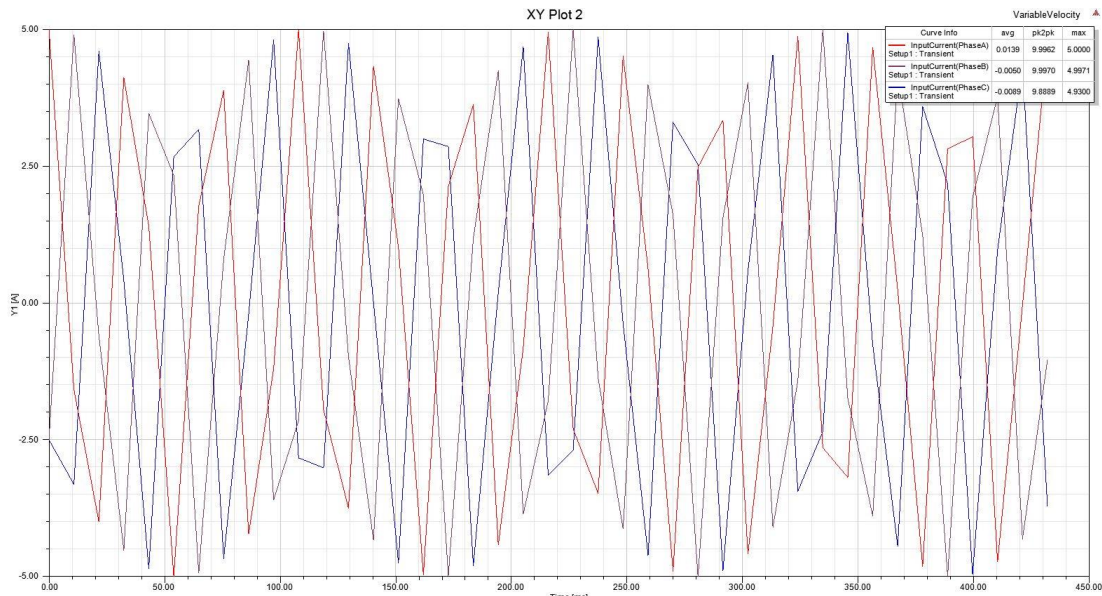


Figure 10: 3 Phase Input Current

The plot in figure 10 was made to ensure that the window of simulation was large enough to provide multiple periods of the sinusoidal current input. Furthermore, it is ensuring that the simulation is accurate enough to approximate a perfect sinusoidal waveform given the accuracy that was used for the simulation.

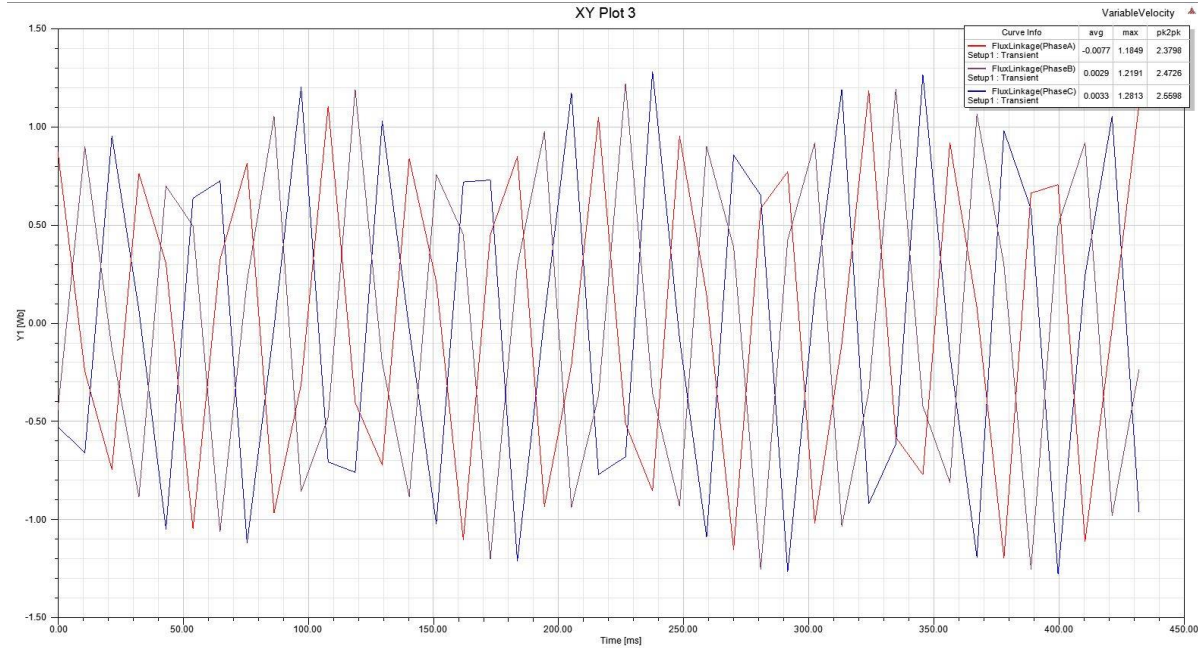


Figure 11: Flux Linkage per Phase

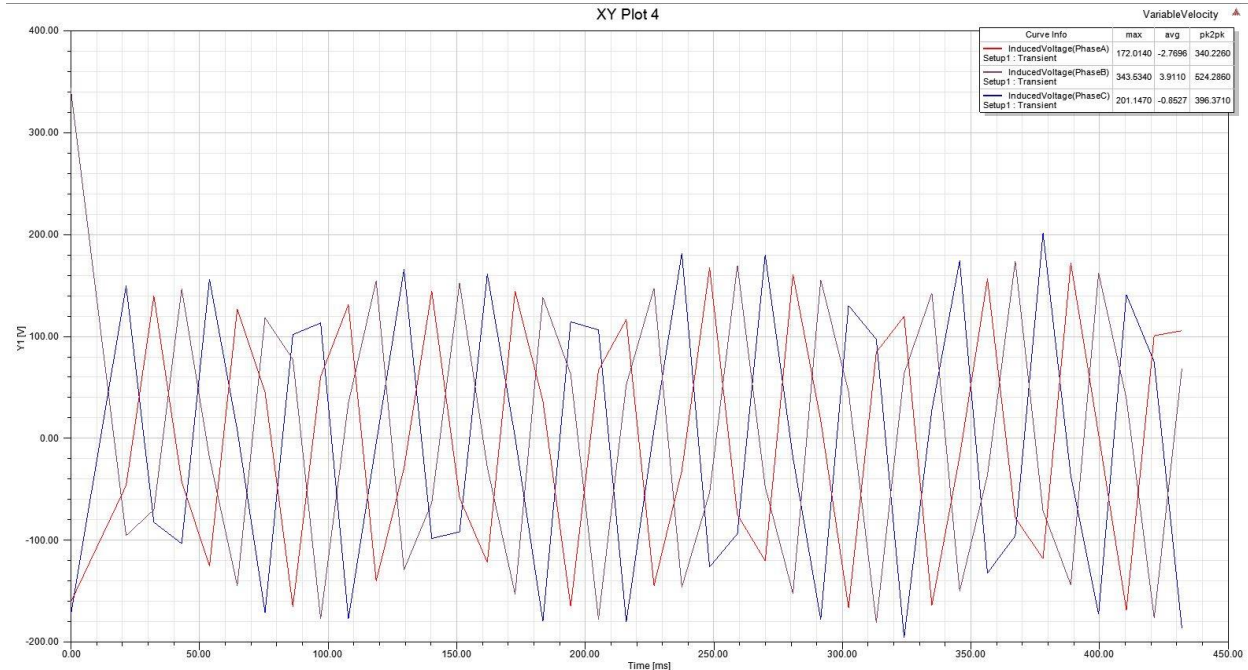


Figure 12: 3 Phase Induced Voltage

The induced voltage, produced by the coil stacks on the stator side, is an important characterization of the SLIM performance since it dictates the rated performance of the SLIM. From the results it can be seen that the induced voltage is sinusoidal and is centered around a voltage of 0V. The legend in the top right corner provides peak values of the induced voltage in each phase which was used in the performance calculations. Additionally, there is error in the waveform showing a varying amplitude in the sinusoidal wave. This is due to the time step not

being detailed enough to simulate a perfect sinusoidal wave. These skewed results were taken into consideration and are a result of reducing the simulation time.

The magnetic, transient domain in ANSYS Electronics uses a simulation method that is based off a band excitation. This means that the user provides the rotor velocity as an input value before simulating, which then returns the force and magnetic field results at the given rotor velocity. This can be seen in figure 13 which shows the rotor velocity input. The value was set at  $V_r = 0.9(V_s)$ , which is indicative that slip has a value of 0.1. The rotor velocity input was set to 0 at the 280ms mark so that force values can be compared at  $V_r = 0$  and  $V_r = 0.9(V_s)$ . The force plot in figure 14 indicates that an excess of losses are present. This is because the levitation force is equivalent at both rotor velocity cases. Furthermore, the thrust force is almost negligible.

It is stated that design 1 is used as the final SLIM design which is not ideal. This was decided since other subsystems require important LIM characteristics well in advance of the FDP deadline. Therefore, it was decided on as a result of the deadline constraint. Design 2 that is proposed has a lot more promise and retains the overall dimensions that design 1 has. Therefore, implementing design 2 and future iterations of itself would not require much recalculation and design work to use this new propulsion system.

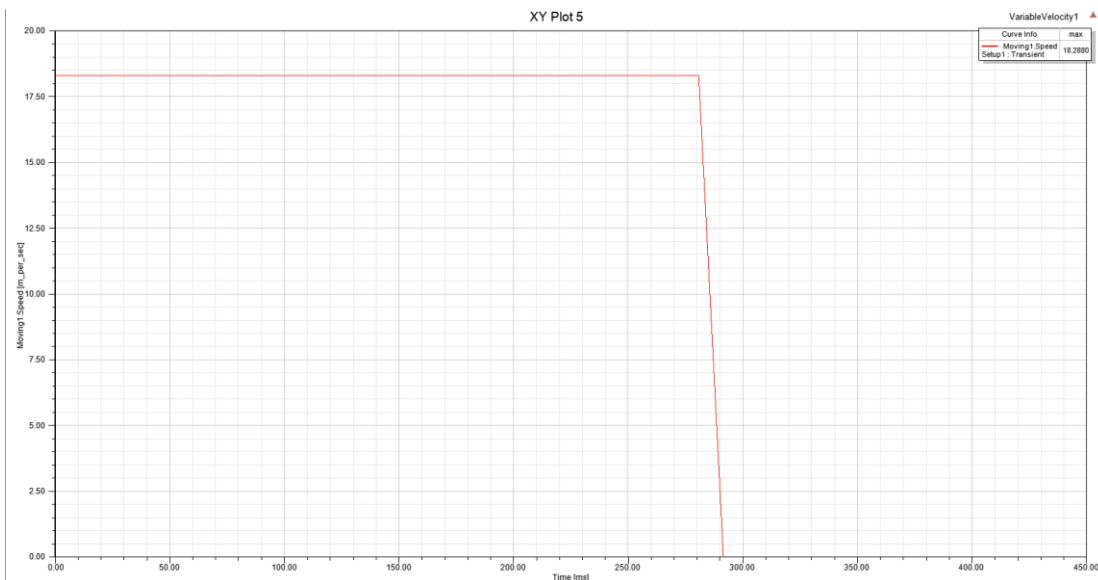


Figure 13: Velocity Vs. Time Plot for Design 1

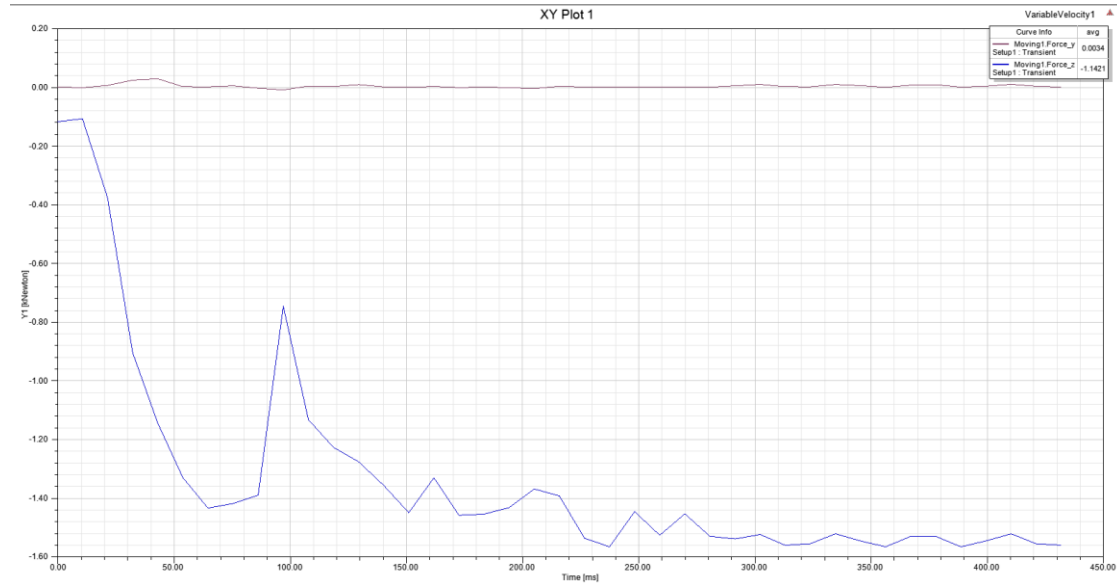


Figure 14: Thrust and Levitation Forces Vs. Time for Design 1

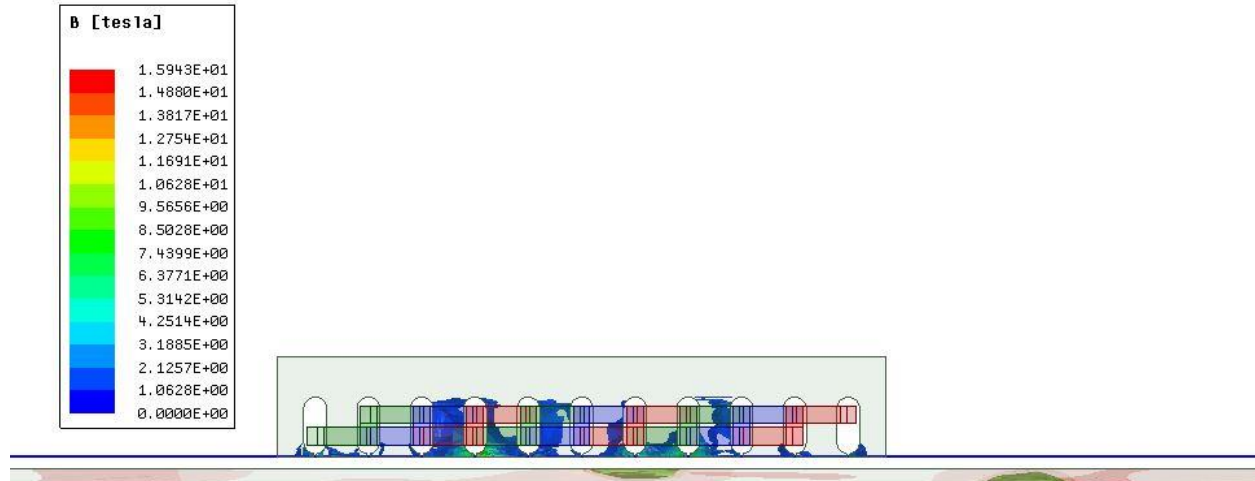


Figure 15: Magnetic Field Density Simulation of Stator Core

The magnetic flux density inside the core is an important parameter of the SLIM design since saturation can limit the output performance of the motor. The saturation point is characterized by a graph and is governed by the material of the motor core. This material was highly debated among the team and a conclusion was made to incorporate grade 50C600 electrical steel as the stator core material. From table 3 below, the max flux density is stated as 1.5T. As a result, the design iterations took into account this limiting value by making sure to not exceed this limit. This can be seen that the flux density is only exceeded in the teeth of the stator core. Although there is saturation in the teeth, it is at a highly concentrated location, which is relatively small in size when compared to the entire volume of the stator teeth. Further improvements will be made to this stator core design by an iterative process to further mitigate the saturation in the core.

GRADE / COATING / DIMENSIONS DETAILS															
Grade	Customer Grade	Coating	Avg. Coating Thickness in (µm)	Insulation Resistance Before SRA (Ωcm²/LA)	Nominal Thickness (mm)	Width (mm)	Length (mm)	Thickness Tol. (mm)	Thickness Tol. (Typical) Micron	Width Tol. (mm)	Length Tol. (mm)	Coil Wt. in MT	Coil ID (mm)	Burr (Max As per IS648) in µm	Burr (Typical) in µm
50C600	M45	C-6A	0.4~1.0	≥0.5	0.50	1000~1200	Coil	± 8% of Nominal Thick.	±15	-0+1.5mm	N.A	3.0~12.0	508±10	≤50	≤20

MAGNETIC & MECHANICAL PROPERTIES															
Grade	Customer Grade	Assumed Density	Core loss at 1.0 T/ 50 Hz	Core loss at 1.50 T/ 50 Hz			Magnetic Flux Density (in Tesla)			Typical Mechanical Properties for Reference					
			Typical	Guaranteed	Typical	Guaranteed	Typical	Guaranteed	Typical	Tensile Strength	Yield Strength	Elongation @ 50mm Gl	Hardness at HV1	Lamination factor %	
			Kg/dm³	W/Kg	W/Kg	W/Kg	2500 AT/m	5000 AT/m	5000 AT/m	(N/mm²)	(N/mm²)	in %	in VPN	Guaranteed	Typical
50C600	M45	7.75	2.06	<6.00	4.15	<2.72	1.62	>1.66	1.71	400±20	270±20	37	130±15	>96	98

Table 3: Electrical Steel Properties for SLIM Stator Core

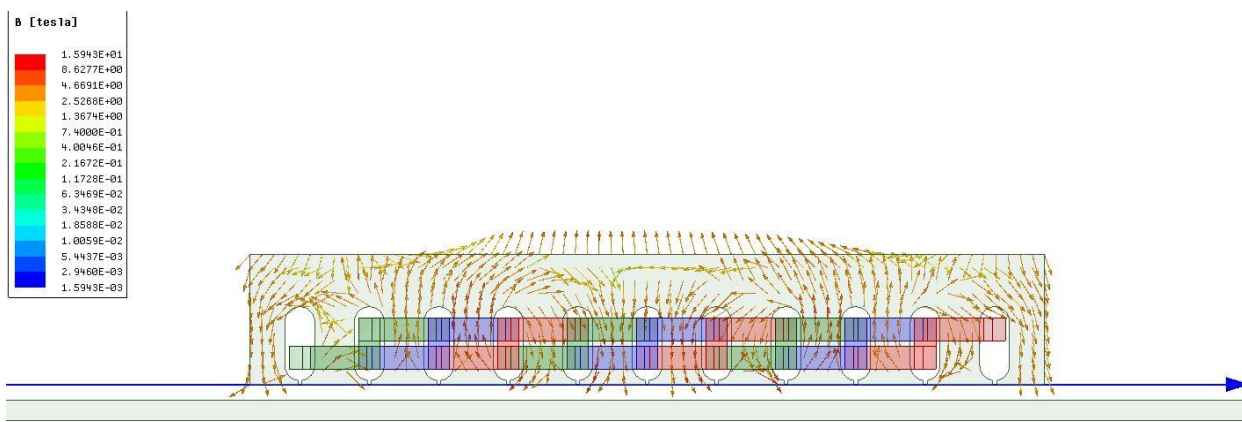


Figure 16: Magnetic Field Simulation of Stator Core

This simulation was created to visualize flux vectors inside the stator core. It reassures the simulation since it provides an accurate vector field model according to solenoid magnetic field theory simulations.

- **Include details on power requirements**

The power inputs for the SLIM are heavily constrained by the on board battery supply. This is a DC supply converted to AC using an inverter. After discussing design iterations for the battery, it was decided that an input of 5A per phase would be used at a voltage of 400 Vac and 60 Hz. As a result, the power input to the SLIM is dictated by the equation:  $P = \sqrt{3} * V I \cos(\theta)$ . This calculation provides an input power of 2.15kW to the SLIM.

- **How the LIM is being controlled**

To grade the performance of the SLIM, the following parameters are heavily measured and analyzed: frequency input, current input, thrust force, levitation force, lateral force, and slip. Only frequency and current are inputs which means they can be varied to alter the performance of the SLIM. The frequency of the current input controls the velocity of the SLIM, and the

amperage of the current input determines the force generated. A live reading of these values will be sent to a motor controller and varied to mimic a desired velocity-position plot for the pod.

## 5.4. Thermal Analysis

### Thermal profiles

- Where, why, and how much heat is being generated and how are we planning on cooling it

The LIM draws small amounts of current from the power supply system. The current design requires 5A per phase for the windings. Note that this will not be the case for the future design. The future iterations will draw very large amounts of current through the windings. For this reason cooling units will be needed in the future. Maximum temperatures produced by the LIM in the current configuration are rather low, therefore, a cooling unit is unnecessary. With the above stated, the following is an analysis of the heat generated by the copper windings in the current configuration; these calculations can easily be repeated for future versions of the LIM:

The thermal analysis begins with the power being supplied to the LIM. The current going through the wires in this example is 5A. Using this current going through wires, the resistance of the wires, the length of the windings, the number of windings in each loop, and the number of loops. Using Joule's Law, the heat generation can easily be calculated as shown below:

$$I = \text{Current}$$

$$R_l = \text{Resistance Per Unit Length}$$

$$t = \text{Time}$$

$$L_w = \text{Length of Winding}$$

$$N_w = \text{Number of Windings/Loop}$$

$$N_l = \text{Number of loops}$$

$$Q = (I^2)(R_l)(t)(L_w)(N_w)(N_l)$$

$$Q = 561.2J$$

This calculation assumes the worst case scenario: there is no insulation between the wires. The 561J will be produced uniformly over the time it takes to accelerate the pod to full speed. This is an average of 78W of heat production per side of the LIM.

Seeing as the windings will be held together in loops, the loops will be coated with an insulating varnish. The varnish will be applied to the outside of the large windings to insulate the copper wires from shock or interference. The varnish will be very thin, and provides very little thermal resistance. The temperature of the large windings are as follows.

$$R_{ins} = \frac{\ln \frac{r_o}{r_i}}{(2)(\pi)(k)(l)}$$

$$R_{ins} = 0.293 \text{ } ^\circ\text{C/w}$$

$$T_h = (Q)(R_{ins}) + (T_c)$$

$$T_h = 70.8 \text{ } ^\circ\text{C}$$

**Where**

$T_h$  = Temperature of Wire

$R_{ins}$  = Thermal Resistance of Coating

$T_c$  = Length of Winding

$r_o$  = Outer Radius of Loop

$r_i$  = Inner Radius of Loop

$k$  = Thermal Conductivity of Coating

$l$  = Length of Winding

With a maximum temperature of 70.8°C, the copper coil will be able to radiate its heat into the ambient conditions of the tube. Some of the heat will also be allowed to conduct into the steel stator. Due to this there is no need for a cooling system in the present model.

## 5.5. Test and Validation

### 5.5.1 Finite length Aluminum Plate Test Rig

Two test rigs have been designed for two separate purposes. The first is a finite length of aluminum plate made to mimic one of the sub-tracks. This setup is useful for both blocked rotor tests and dynamic tests. From the blocked rotor test, short circuit current at normal voltage, power factor on short circuit, total leakage reactance, and starting torque of the motor can be found. This setup is also useful for testing dead zones and breaking characteristics. An important feature of this setup is portability since the length was designed to be just long enough to measure the first second of operation. Truly this is important for local testing, but also for when testing needs to be done elsewhere, such as the Hyperloop track. A CAD design was not made for this design because it will be designed to mimic the Hyperloop subtrack and any inconsistencies will produce losses or error in results.

### 5.5.2 Flywheel Test Rig

The second design is a flywheel test rig which will be used so that the LIM can create a force on the plate and have an infinitely long section of track relative to its position. This is useful for testing durability, varied duty cycles, thermal analysis in a practical setting, and non-linear breaking. The potential errors for this design is the residual eddy currents that remains in the secondary aluminum plate. This will likely create losses that must be tested against and accounted for in the practical results. A CAD model can be seen of the flywheel in figure 17. This will be coupled with multiple sensors fixed to the frame which will help characterize additional features. For examples, temperature probes will be used to conduct thermal tests on the stator core and reaction plate.



Figure 17, Flywheel Rig

## 5.6. FMEA

Discussed below are the potential failure modes for the SLIM and what uWinLoop has done to address them.

### 5.6.1 Overcurrent Draw

To protect the SLIM during operation, it is imperative that a control system be put in place to prevent overcurrent draw. To accomplish this a 3 phase circuit breaker rated to trip when the SLIM current draw exceeds the rated current input. This ensures that the SLIM windings do not overheat and cause permanent damage to material properties or even melt wires. In an extreme case, the heat generated by a faulty SLIM could even cause a fire. With a circuit breaker in place, this will be prevented. It is important to choose a circuit breaker that has short-time delay (STD). Choosing an appropriate STD depends on the current draw characteristics are full load. This will occur in the first few seconds of operation before a cruising velocity is reached. Since the STD value is generally in the range of 6-30 cycles, it is important that the rated circuit breaker current not be surpassed if the 6-30 cycles does not contain the time it takes for the SLIM at full load.

To protect the rest of the control circuit in the case of a short circuit or fault, 3 fuses were implemented. Each individual input line coming from the battery is fused at the rated current output for the battery. This will prevent any extra current draw and is designed as a single use function. This is a result of fusing being much cheaper than circuit breakers.

### **5.6.2 Excessive heat generated by the stator**

It is important to continuously validate that SLIM is not overheating or surpassing the expected heat output. To accomplish this, multiple temperature probes will be used to measure the heat output at points of interest. These will be strategically placed in locations that have high flux densities from the simulations using ANSYS Electronic.

### **5.6.3 Excessive heat generated in the subtrack**

The Hyperloop competition states that the subtrack is not allowed to be externally heated by a delta of 30 degrees Celsius. The temperature of the subtrack will be measured after we pass each location.

### **5.6.4 Minimum air gap breach**

The air gap is important to maintain since it is an important characteristic of SLIM performance. Since the air gap for the SLIM design is generally in the range of 0-10mm, this is a very important distance to monitor since a slight external bump or error could cause the stator core to scratch the sub track. This is because the core is made of cold rolled steel and is harder than the aluminum sub track material. To assure that this scratching is not possible a mechanical lock is put in place at a value of 0.1 inches. This is done by the stabilizer sub system.

## **5.7 Future Design**

A large amount of time was dedicated to improving the performance of the SLIM with variations in the design characteristics. To accomplish this, much time was invested in detailed theoretical calculations. This is a good place to start researching the effects that certain variables have on one another. For example, a summary was made for varying parameters and their benefits to SLIM performance characteristics which can be seen in table 4 .

Parameter	In case of increasing	In case of decreasing
Airgap (g)	Larger magnetizing current Larger exit-end losses	Larger goodness factor Larger output force Larger efficiency
Secondary thickness (d)	Larger goodness factor Larger starting current	Larger secondary leakage reactance
Secondary resistivity ( $\rho_r$ )	Smaller end effects	Larger goodness factor Less secondary loss
Primary core materials magnetic flux density ( $B_1$ )	Increases efficiency Increases power factor	Reduces thrust
Number of poles (P)	Smaller end effects	Larger secondary leakage reactance
Chamfering of primary core ( $\alpha_c = 5^0 - 45^0$ )	Reduces end-effect Reduces Dolphin effect Thrust improves	Increase in transversal edge effect Increase in end-effect
Tooth width (w)	Larger leakage reactance	Larger force Larger efficiency

Table 4: Effects of parameters variations on SLIM performance

In this section, future design concepts of SLIM will be discussed along with the sources of error in design 1. This will then be compared to design iteration 2, which is a proposal for the new design. This will then be discussed further since improvements are still necessary.

As stated earlier in the propulsion section, the user provides the rotor velocity as an input value before simulating, which then returns the force and magnetic field results at the given rotor velocity. Although this concept is clever, it complicates the design process for SLIM. In a practical setting, the SLIM rotor velocity is an output, therefore some reverse engineering must be done to characterize the velocity versus position plots and any others that are important to SLIM performance. Unfortunately the ANSYS software does not provide any plots for this so the solution to this is solving for each data point for the given slip range.

Slip is defined as the ratio between synchronous velocity and rotor velocity. As the duration of SLIM operation increases from a time of zero, the rotor velocity naturally increases to match the synchronous velocity. It is important to note that this only occurs when the losses are small enough for the SLIM to overcome at a slip of 1. Therefore, the thrust force increase as slip approaches 0 and then decrease once it is very close to 0. These results match LIM theory and can be compared to the plot shown below in figure 18. This reassures the simulation and allows for an optimized slip value to be determined for use at each acceleration profile.

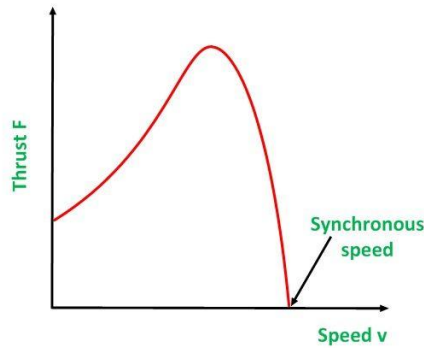


Figure 18, Thrust Vs. Synchronous Speed

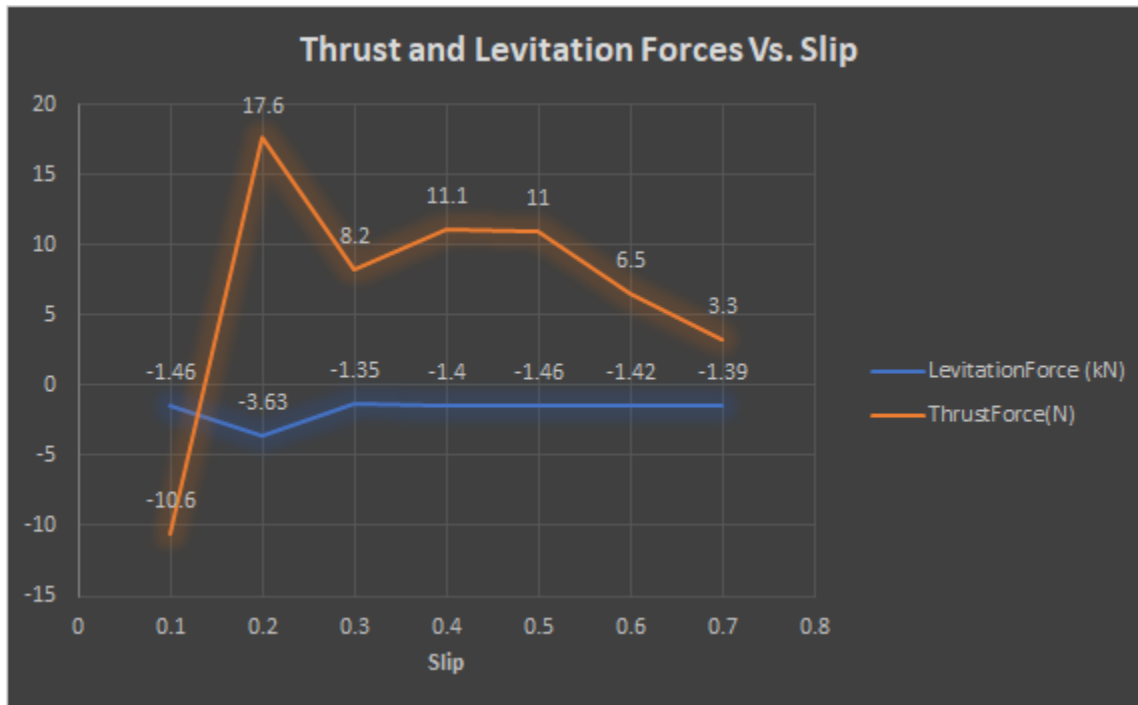


Figure 19: Thrust and Levitation Forces Vs. Slip of Design 2

Due to the lack of resources, velocity versus position graphs were not plotted. These can be achieved by designing a slip vs time curve that will be achieved by varying the frequency with time to ensure that the thrust at each point in time matches the simulated thrust curved.

It is important to note the obvious issue with the plot shown above in figure 19. It is evident that the levitation force is negative, resulting in the SLIM being pulled towards the subtrack. This is not acceptable since the design constraint of the provided subtrack from Hyperloop doesn't allow a SLIM to be suspended by magnetic levitation. Therefore, the simulations must provide a repulsive force to allow for SLIM levitation. It is characteristic for SLIM operation to have an attractive force at low speed operation. The error occurs in the high-speed operation, which does not show the curve intercept the x axis and become repulsive. This property will be further

studied and simulated to ensure that the levitation force has both repulsive and attractive values in the slip range.

Attempts at solving this issue will be made by testing the following cases:

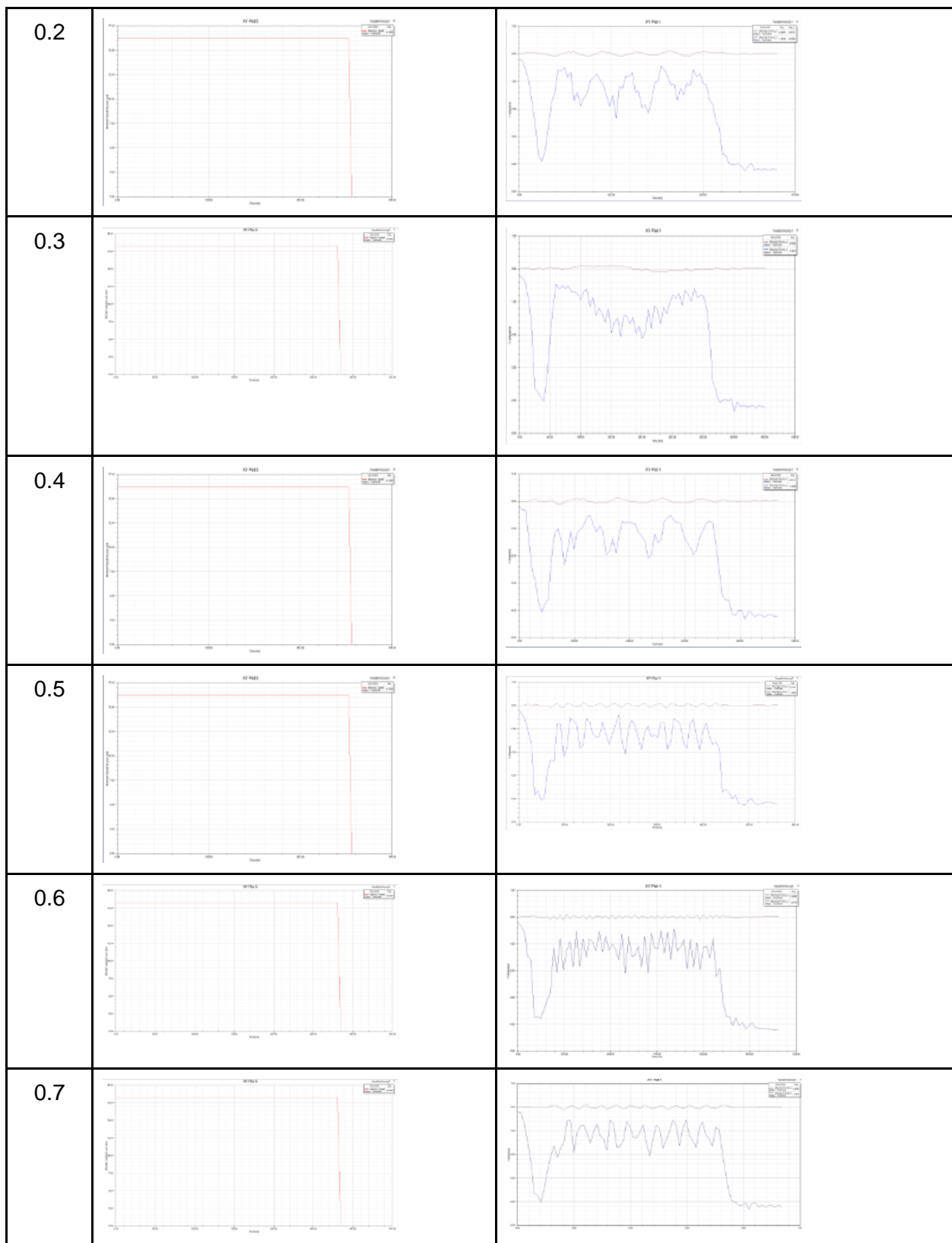
- Thinning the stator teeth until saturation point
- Decreasing air gap until minimum allowable air gap is reached
- Increasing chamfer angle until saturation point
- Increasing number of poles in the stator
- Adjusting the current to turns in the winding ratio

As a result of the attractive and repulsive levitation force curve for SLIM, it will be necessary to use an initial propulsion system to get the pod to critical speed before activating the SLIM. This could be something as simple as a friction drive. Further testing must be done to find the critical point at which SLIM should activate so that the repulsive force will cancel out the net force of the pod weight. At this point the friction drive can be deactivated or work in unison with the SLIM. These calculations and simulations will be conducted once the open issues with SLIM have been resolved and an optimized SLIM is realized.

To improve the speed at which these simulations can be conducted, 2D designs for SLIM will be investigated using ANSYS Electronic. Currently each simulation takes approximately 10 minutes with relatively accurate time steps. If variable sweeps were to be conducted, it would take  $x$  amount longer if there were  $x$  steps in the sweep. For example, to optimize the air gap it is necessary to test a wide range of air gap values and observe its effect on performance characteristics. To do this one might sweep the air gap through 5 values which would increase the simulation time fivefold. Additionally, the ANSYS Electronic licenses at the University of Windsor limits the number of usable cores to 1. This makes it difficult to improve upon the simulation time without making changes to the design setup. As a result, 2D designs will be used to optimize the SLIM design and the 3D design will be used to simulate the optimized value with very high accuracy.

Table 5, Rotor/Slip Table

Slip	Rotor Velocity	Force Output
0.1		



## 6. Braking

### 6.1. System Overview

The pod is designed to reach maximum velocity of 139 m/s. Once that speed had been reached the pod had travelled 500m of the total travel distance. In order for the pod to come to a complete and controlled stop a reliable braking system was needed.

The braking subsystem was designed to be robust and fail safe in an event of an emergency. In order to achieve these objectives the team decided to incorporate two different systems for braking: Friction braking and LIM Braking. During normal operations once the pod has reached a maximum speed of 139m/s both braking systems would activate simultaneously to decelerate the pod to a complete stop. The friction braking system is designed such that the default position is “brakes applied”. In case of an emergency, the contact braking mechanism was design to stop the pod from its maximum speed on its own. In the current design, the LIM will only be responsible for a small portion of the overall braking force.

### 6.2. Friction Braking

The friction braking would be the primary source of braking and so it needs to be reliable in an event of an emergency where all power to the pod is cutoff or the pod requires an emergency stop.

The friction brakes are located at either side of the middle of the I-section, at both the front and back of the pod, making a total of four brake pads. The friction braking system is a unique mechanism, in the sense that they are a self-locking system. Traditionally this system is used for applications where a very fast acting fail safe system is needed. It is usually employed in lifting devices such as elevators, cranes, mobile scaffolding for buildings and the largest drawbridge in the world in the Millau Viaduct. Through some modifications and a rigorous optimization process, the self-locking mechanism has been tailored to the hyperloop application. This allows for a full scale friction braking system that is capable of stopping the pod fully on its own. This is achieved by requiring little force to engage the brakes as an input, while having a large braking force as an output.



Figure 20, Braking With Support Structure

### 6.2.1. Operation and Performance of Friction Braking

The braking effect is produced by squeezing two triangular shaped aluminum 5052-H32 blocks lined with organic braking material, against the I-beam. The brake pads are 11.5 inches long, 2 inches thick and 2 inches wide. The actuation is produced by a spring that can deliver a force of 1000N when at the end of its travel. The wedge makes contact with the beam (braking wedge), is cocked back by a linear actuator, which is powered by an electric 12V DC motor. When power is cut off to the actuator, the compression spring moves the braking wedge forward. The second wedge that does not contact the beam (fixed wedge), is fixed during the actuation and braking phases of operation. As the spring moves the braking wedge towards the fixed wedge, the braking wedge moves towards the I-beam at the same time due to the angle between the wedges. To ensure a smooth engagement as the braking wedge moves towards the beam, the actuators are allowed to slide via a small slider and track located on the braking frame. This slider contains four small centering springs.

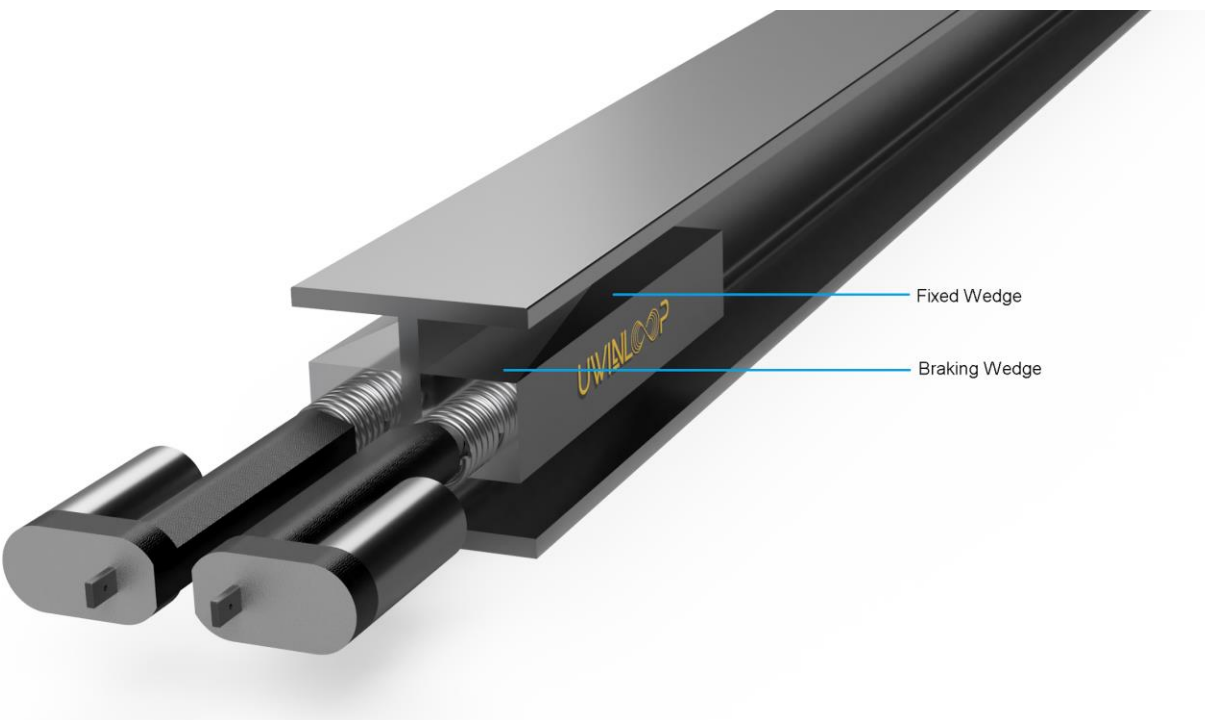


Figure 21, Braking Core

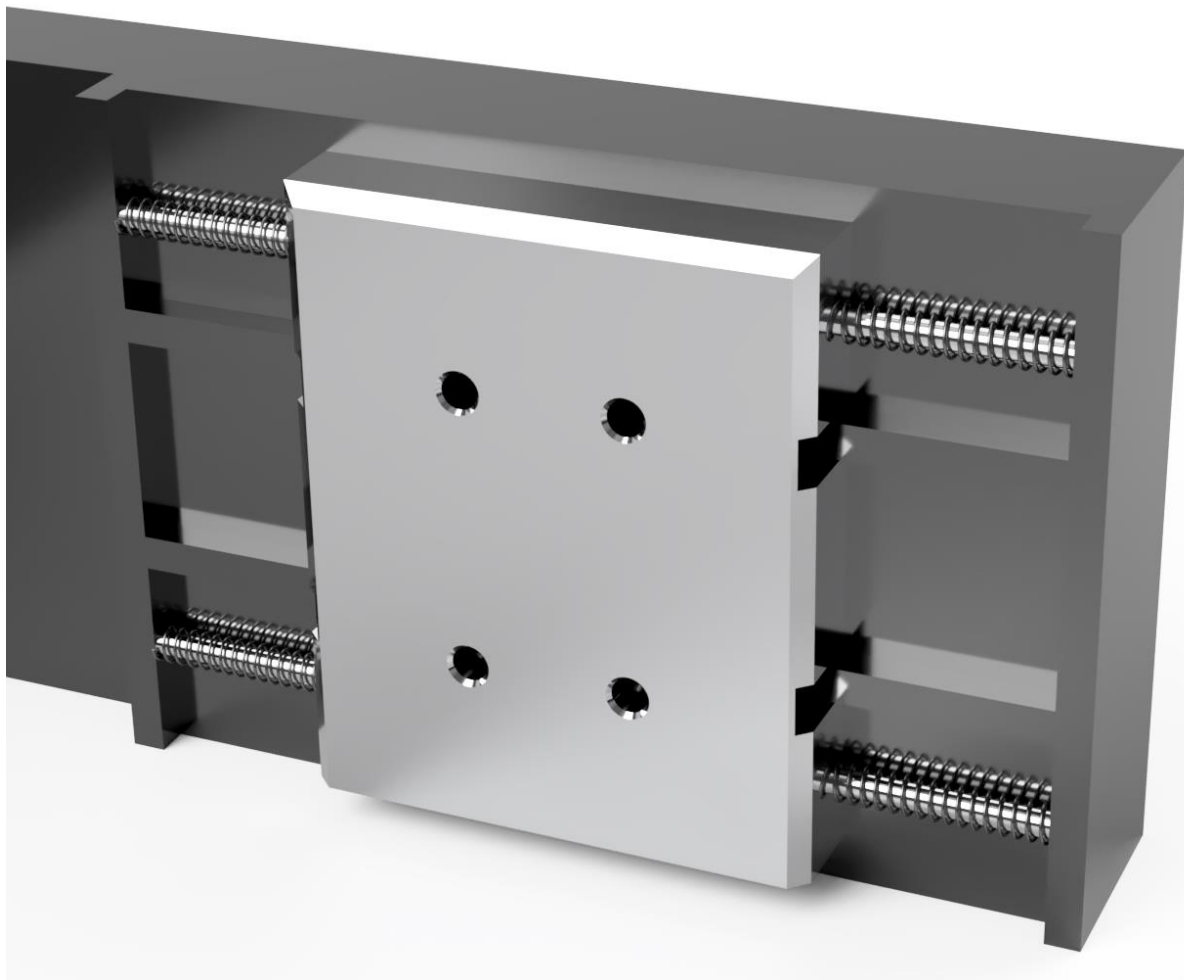


Figure 22, Slider Mounted To Actuators

A small chamfer angle on the leading edge that contacts the beam of the braking wedge ensures that the rear of the pads contact the beam before the fronts do. This prevents the braking wedges from locking up abruptly due to any possible misalignments that may be present in track. At the time of the first contact for the brake pads to the beam, the spring will produce 1000N of force. A force of friction is created by the normal force of the braking wedge and the beam, which is a result of the normal force between the two wedges. The force of the friction created by the system will draw the braking wedge in, causing it to self-lock. The brakes combined will be able to produce a maximum braking force of about 11kN.

Once the basic forces were evaluated in the system, it was discovered that the braking force will impact the speed and vice-versa, in a closed loop system. This was solved for using an iterative solution similar to that of a fixed point iteration. This model was done in excel using a small time-step. Using that solution, the design was optimized until all requirements were met. This was done by creating a calculator model to output. The braking force given inputs such as material selection, geometry and initial spring force. The result is a system that can stop the pod from 139 m/s to 0 m/s in about 320m, with a maximum deceleration of 3.1g.

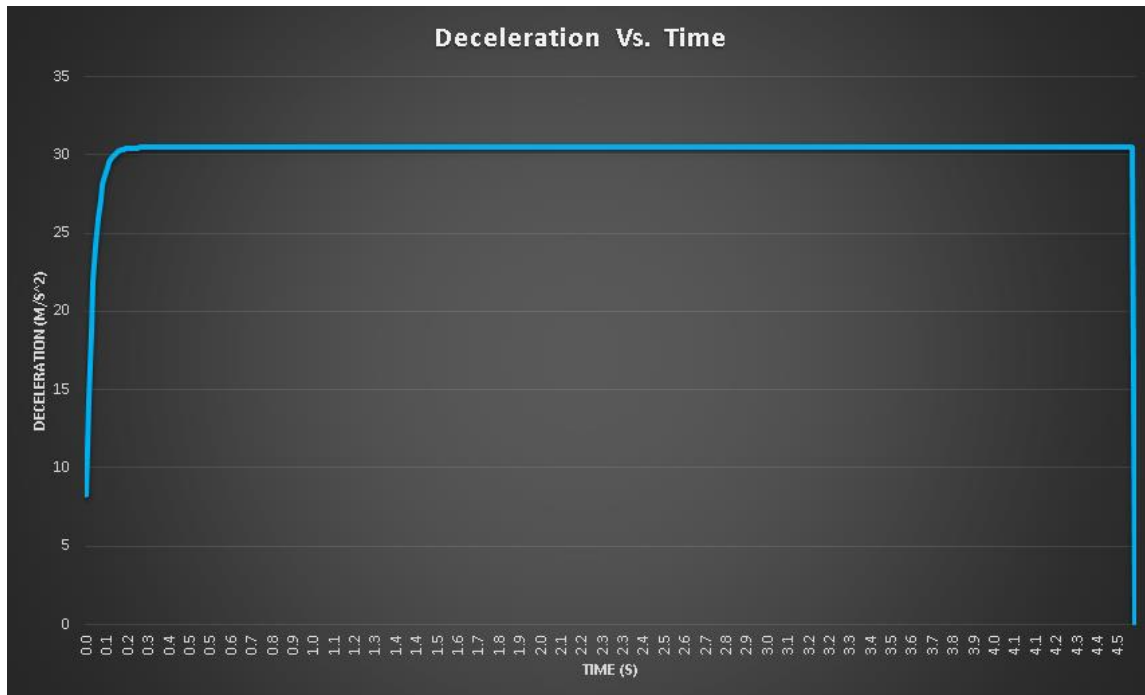


Figure 23, Deceleration Vs Time Graph

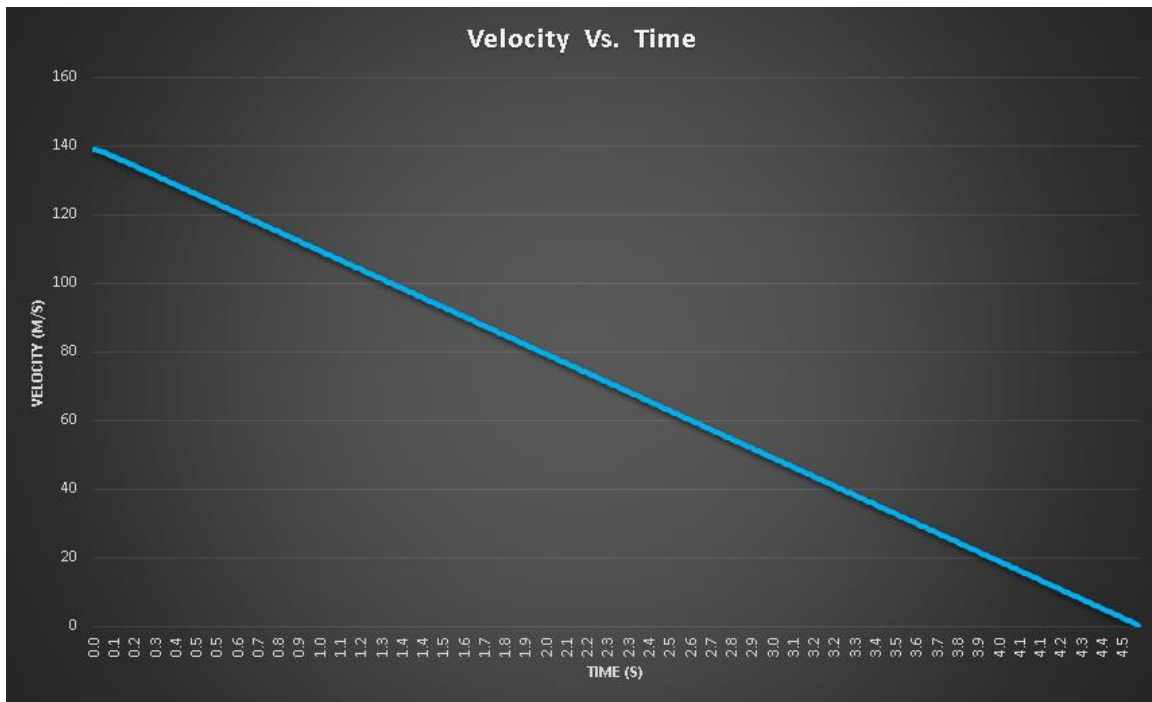


Figure 24, Velocity Vs Time Graph

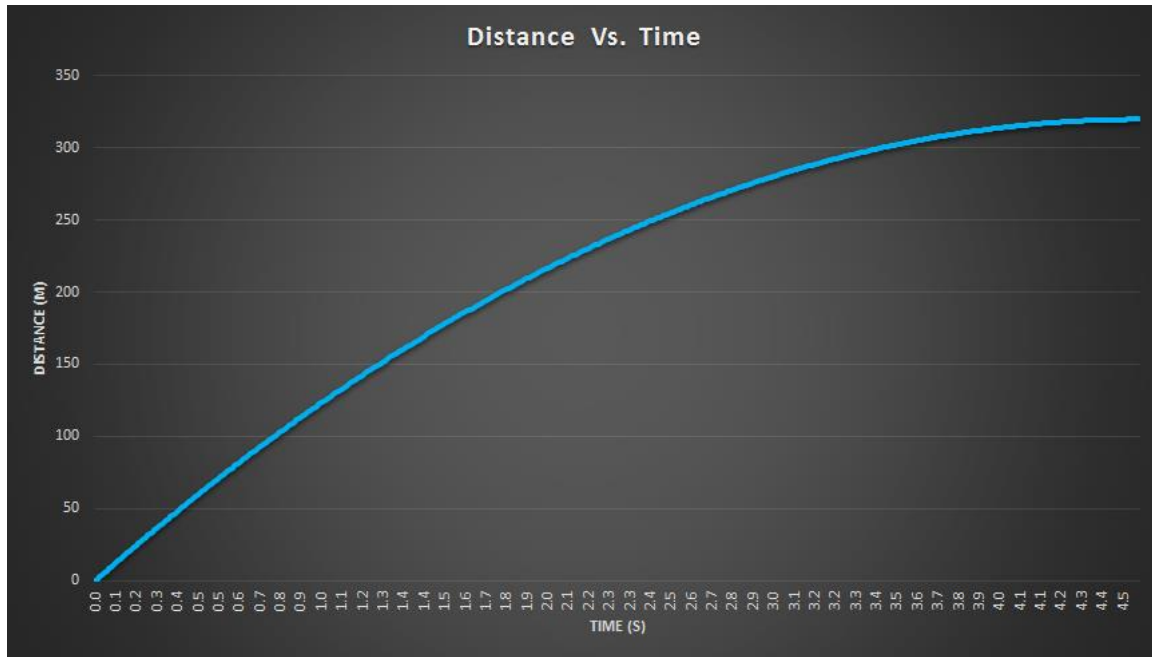


Figure 25, Displacement Vs Time Graph

When it is time for the brakes to be released, the second set of four small actuators will pull the fixed wedges out, away from the beam. This will allow the braking wedges to be retracted by its linear actuators. There are support plates above and below the wedges to keep them level in the vertical plane. These plates also support the wedges when it is time to retract them.

Even though the brakes are being applied symmetrically along the I-beam cross section, high forces are being applied. So it is important to ensure the stresses involved will not exceed the elastic region of the aluminum I-beam. The simulation has been set up in transient structural mechanical workbench, within ANSYS V19.2 Workbench, to analyze the brake pads and cross section of the beam. This simulation is done as the engagement contact begins, through the entire duration of braking which will last 4.57s, if only friction braking is used. However the simulation images below are from just after the brakes have achieved their full braking force. This is the moment in time where the largest stresses will exist. The simulations have also been simplified to show only the beam and the brake pads to minimize meshing and simulation time. The beam was fixed accordingly and two frictional planar joints were created on each side of the I-beam. The proper forces were applied to the pads and the joints, along with the projected velocity profile. The maximum yield strength of aluminum T6-6061 before plastic deformation will occur is at least 240 Mpa. The maximum principal stress seen in the beam will be 0.49 Mpa and maximum equivalent (Von-Mises stress) will be 1.05 Mpa. This means that the center beam will not be damaged in the case of emergency braking.

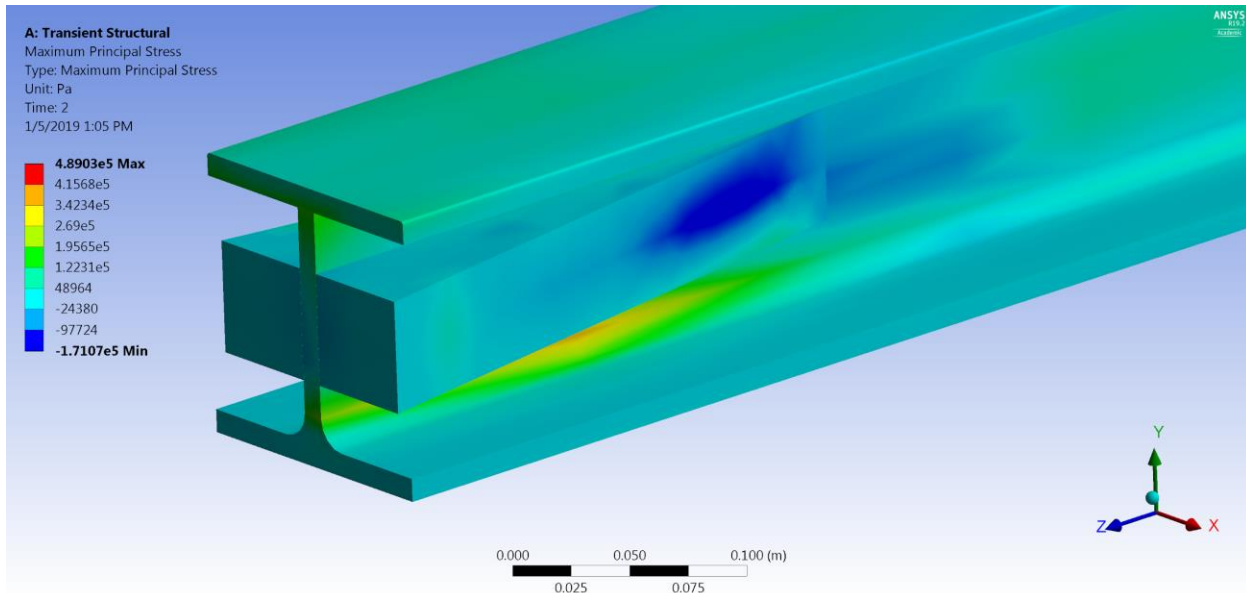


Figure 26, Maximum Principal Stress In Pads

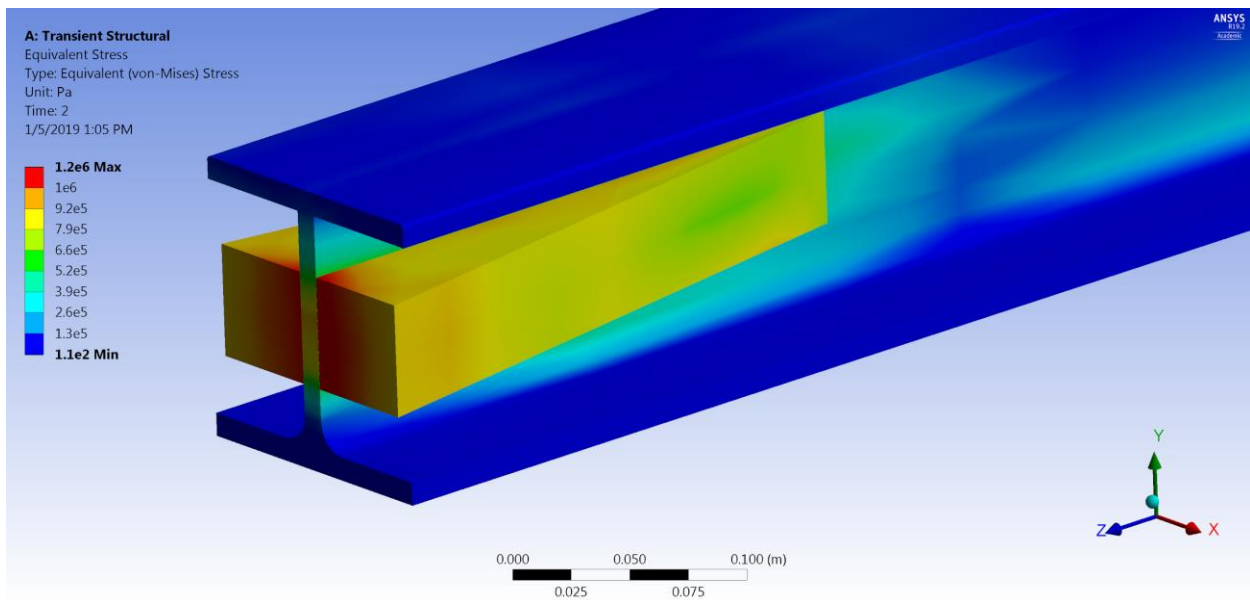


Figure 27, Maximum Equivalent Stress In Pads

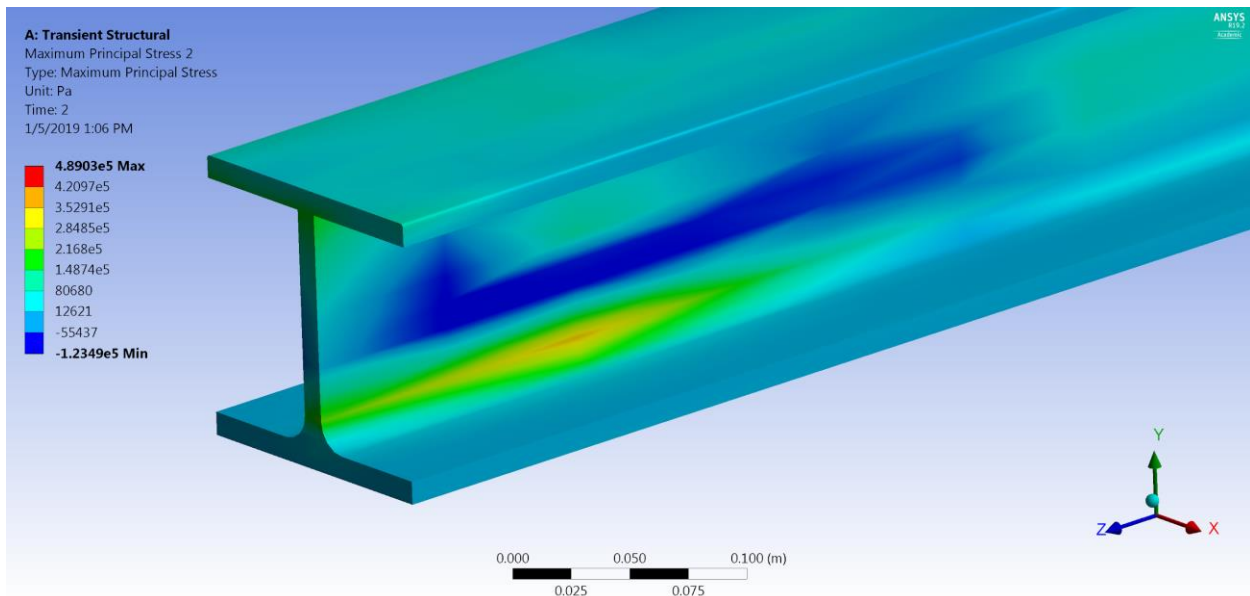


Figure 28, Maximum Principal Stress In Beam

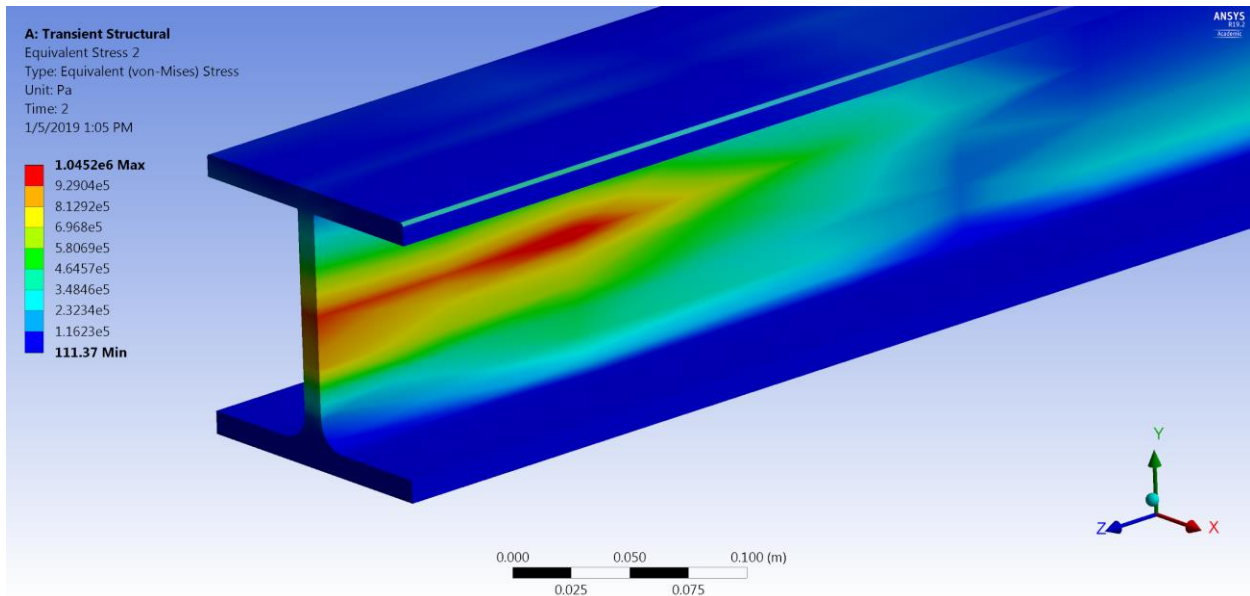


Figure 29, Maximum Equivalent Stress In Beam

### 6.2.2. Thermal Analysis and Material Selection for Friction Braking

The forces acting on the beam are very high as stated in the performance section. For this reason it is important to conduct analysis of the thermodynamics of the braking system in the worst case scenario. Assuming the worst case scenario, in which the pod's maximum kinetic energy is transferred to the brake pads, the temperature increase is as follows;

$$m_{pad} = \text{Mass of Pads}$$

$$c_p = \text{Specific Heat of Pads}$$

$$T_h = \text{Hot Temperature}$$

$$T_c = \text{Cold Temperature}$$

$$v_{pod} = \text{Velocity of Pod}$$

$$N_{pad} = \text{Number of Pads}$$

$$(m_{pad})(c_p)(T_h - T_c) = \frac{(m_{pod})(v_{pod})^2}{(2)(N_{pad})}$$

$$T_h = 962^\circ C$$

This value is the uniform temperature of the pads. In reality this value will not be uniform as the brake liners themselves will heat up the most. Another simulation was conducted in ANSYS to simulate the temperature distribution in the pads. This was done using the transient thermal analysis workbench in ANSYS 19.2. The areas in red in figure X, represent temperatures around 1010°C while the blue represents around 58°C. The liner is going to be made of a compound braking material, ideally a Kevlar based fiber pad, with ceramic filling. This material was chosen for a few reasons. One being that the brake pads must wear rather than the beam itself. Since the pads are lined with Kevlar, which is softer than the beam, they will degrade before the beam ever does. Secondly, the Kevlar material has very good frictional and heat properties. The material grade still has to be explored a bit further in the future however right now, we are targeting an HH friction grade (0.55-0.75 coefficient of friction). HH grade Kevlar/ceramic material is able to withstand temperatures of up to 1400K. These materials are available as both pads and as liners. The braking wedges are made of a grade of aluminum (5052-H32) that is 35% softer than the beam. This is to allow the wedges themselves to act as a large heat sink and for safety.

In the event the brake liner degrades faster than expected and the wedge underneath were to contact the beam, there must be no damage to the beam. Finally the fixed wedge will be made of 316 stainless steel. It was selected because of its low coefficient of friction between itself and the braking wedge. The brake liners will be able to operate at the temperatures shown by ANSYS, and the aluminum will be able to operate without melting. With that stated, there is no need for a cooling unit for the brakes. In the future, a cooling unit could be added if for some reason the braking load increases or simply increase the number of pads on the pod. A cooling unit would be implemented into the braking wedges as a series of small copper tubes filled with a cooling agent, which would be cycled through using a small closed hydraulic system.

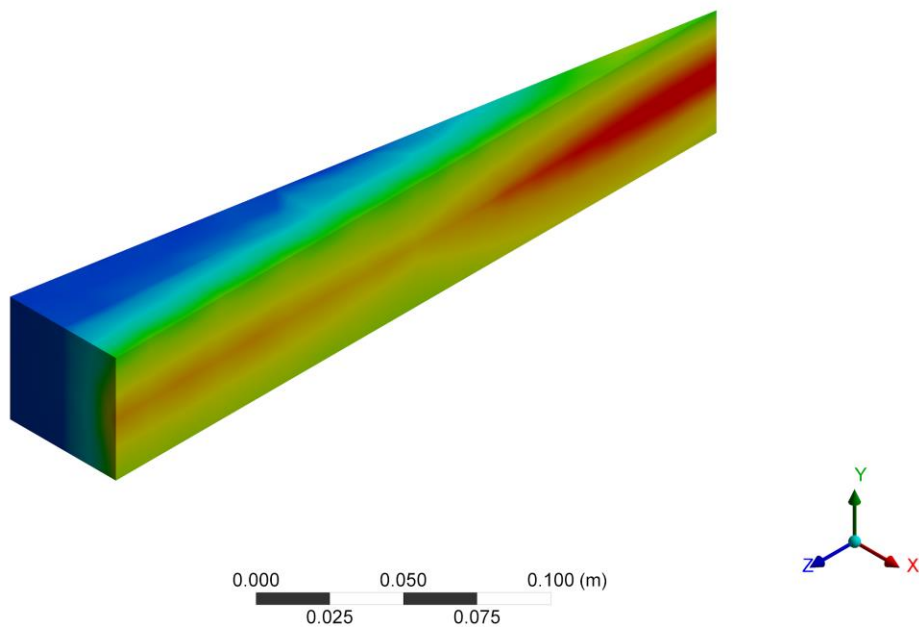


Figure 30, Thermal Analysis of Brake Pad

### 6.2.3. Testing and Validation

The braking mechanism itself will be built and tested on uWinLoop's flywheel test rig. Here the brakes will be tested to ensure that;

- The brakes engage properly
- The brakes stay engaged on their own
- The brakes are self-locking
- The braking force matches calculations (using force gauges)
- The stresses match the ANSYS stresses (collected by strain gauges)
- The brake pad temperature matches the ANSYS results
- The brake liner material does not degrade unexpectedly
- The brake liner material (see below) produces expected drag force
- The release method works to properly disengage the brakes
- All failsafe systems (see FMEA) work properly
- The frame is able to withstand braking forces (see frame section)

Additionally, simple friction experiments will be conducted to ensure the material that is being chosen for the liner meets our requirements. This is the key to the friction system and therefore it must be validated extensively. A full study will be conducted to determine the best possible braking material via experimentation. Vibrational analysis will also be performed on the flywheel to ensure the brakes perform under these conditions. If any of the above fails, the braking system will be modified accordingly. The positioning and strength of actuators to engage/disengage the system is also something that can easily be changed if needed.

All CAD models will be further refined based on the results from the flywheel and experimentation. If any of the above parameters need to be changed they will first be simulated in ANSYS to ensure values are reasonable. A prototype will then be built to test the theory presented by the CAD analysis. If modifications are made physically while testing/experimenting, these will then be re-validated using simulation software such as ANSYS. This process will be repeated until all unknowns or potential concerns are addressed and all experimental and theoretical results coincide within a reasonable margin of error.

If for some reason the friction braking system does not self-lock as predicted, or the forces generated are not great enough to stop the pod as required during the testing of the system here at the University, uWinLoop has also developed an EC braking module (not discussed in this report) that can replace the friction braking system as a failsafe if needed.

#### 6.2.4. FMEA

Discussed below are the potential failure modes for the brakes and what uWinLoop has done to address them.

Total Loss of Power - The braking system is in a default “engaged” position. Linear actuators hold the brakes back in the disengaged position. In the event of a total loss of power, the actuators will shut down, allowing the springs to engage the brakes.

Partial Loss of Power/Actuator Malfunction - In the event that one of the actuators does not release properly, or that one is released prematurely, power to all of the actuators will be cut, forcing all of the brakes to immediately engage. Simultaneously the LIM will be powered into the braking configuration. This will be monitored by simple proximity sensors mounted to the braking frame, to determine which braking wedges are engaged. If only one proximity sensor indicates the engaged position, all of the brakes will immediately engage. This will be monitored throughout the entire run and can stop the pod during any portion of the run.

Brake Pad Material Fails - The braking wedges will be made of a softer grade of aluminum. Even though the brake liner will be tested and validated for performance and that there should not be any performance changes in a vacuum, there must be a backup. In the event that the liner fails for some reason, the aluminum will make contact with the beam. Seeing as aluminum-aluminum has a high coefficient of friction, the wedge itself is capable of acting as a brake while not damaging the beam. Given that some wear is expected in the brake liners, the brake pads will be allowed to coast horizontally as the center of the braking wedge moves closer to the beam. This is achieved by using the small sliders on the back of the braking wedge actuators.

### 6.3. LIM Braking

#### 6.3.1. Performance of LIM Braking

The performance of SLIM being used as braking is purely theoretical at this point in time. It is proven as a viable solution to use a phase-reversed SLIM to aid in the breaking of the pod since switching the phasing via the control circuit in figure 5 is very responsive. Further testing and simulating needs to be done to ensure that the SLIM will not be overworked which can cause excess heat and possibly permanent damage to the motor. Ideally the SLIM thrust performance, when it is in the forward mode, will mirror the similar characteristics of the SLIM in the phase-reversed configuration. For example, the SLIM will provide a much larger breaking force at high speeds rather than low speeds. This is similar to the forward configuration which has a large thrust force at high speeds.

### 6.3.2. Thermal Analysis for LIM Braking

As stated above the performance of each SLIM during braking will match the performance during the propulsion phase. The amount of heat generated during the propulsion phase is very small, which will create relatively low temperatures, such that there is no cooling unit needed. The same applies for the braking phase of the LIM. The linear induction motors will be run in reverse for the duration of braking. The heat generation of the LIM will be negligible due to the low heat production during the propulsion phase.

### 6.3.3. Testing and Validation

Testing and validation for the phase-reversed SLIM will be identical to that of the regular state of SLIM. This will include tests on the flywheel and finite length of subtrack. The principle of testing will be very similar, the only difference being the rotor velocity must be simulated. This will be done on mainly the flywheel, assuming that the residual eddy currents prove to not be an issue when analyzing results. To simulate the rotor velocity of the SLIM, the flywheel will be manually spun to a speed matching that of the current design rotor velocity. At this point, all suitable braking tests can be conducted. This includes the time it takes to reach a full stop, levitation force measurements, and thrust force measurements. A difficulty with this setup is that it does not account for the full mass of the pod which will carry a lot of inertia. This will be accounted for in a braking model that is compared to theoretical results to validate theoretical calculations.

#### 6.3.4. FMEA

Discussed below are the potential failure modes for the brakes and what uWinLoop has done to address them.

**Deadband Reduction** - There is a distinct deadband that occurs when the control circuit of the SLIM activates the contacts to reverse the winding phases. This will change the direction of thrust force in the opposite direction. Since this will be controlled in the controls subsystem, it highly depends on the response time and the timing of the switching operation. Evidently, it is important to reduce the deadband to a timeframe that is as small as possible and acceptable. This will ensure that the SLIM operation is always in control from the controls subsystem. To accomplish this, voltage control will be implemented to perfectly synchronize the phase reversal for SLIM.

**Excessive heat generated by the stator** - It is important to continuously validate that SLIM is not overheating or surpassing the expected heat output. To accomplish this, multiple temperature probes will be used to measure the heat output at points of interest. These will be strategically placed in locations that have high flux densities from the simulations using ANSYS Electronic.

**Excessive heat generated in the subtrack** - The Hyperloop competition states that the subtrack is not allowed to be externally heated by a delta of 30 degrees celsius. An infrared sensor will be used to actively measure the heat generated inside the subtrack. This will be placed directly at the rear of the SLIM to ensure that the heat does not exceed this constrained value.

## 7. Stabilizers



Figure 31, Stabilizers

### 7.1. Overview

The vehicle will have to overcome impulse of the propulsion system, pitch during both acceleration and deceleration, yaw and roll during turning, and any vibrations due to roughness of the rail and airflow. The linear induction motor of the vehicle is very sensitive to displacement, thus a consistent distance between the propulsion unit of the vehicle and ground have to be enforced.

The stabilization system is then developed to achieve all above requirements, and the stabilizers are broken down into two modules: (1) Lateral Control Module (LCM), (2) Vertical Control Module (VCM).

### 7.2. LCM

The LCM was designed specifically to control the yaw of the pod, and dampen any lateral oscillation. Because curvature of the test rail is very small, only a light load is to be expected. However, vibrations from surface roughness, air flow, and potential construction flaws of the rail is still considerable.

### 7.2.1. Structural Design

The LCM consists of a total of four identical assemblies arranged at the front and rear of the vehicle, with two assemblies on each side as one pair to clamp the web of the track. The major components of the assembly are a wheel, an arm, and a spring-damper unit. All metal components are made of aluminium. The wheel is large enough to sustain the high velocity of the vehicle. It is attached at one end of the arm with the other end hinged on the frame of the vehicle, allowing rotatory motion of the arm around the pivot. A spring-damper unit is also mounted on the frame and connected to one third of the arm.

When the vehicle experiences any lateral forces and vibration, the arms stretch and contract and so does the spring-damper unit to absorb and dissipate the energy. Therefore, any lateral instability can be minimized to keep the vehicle running smoothly. The LCM also prevents any yaw motion and keeps the vehicle centered on the track.

### 7.2.2. Stress analysis

The LCM will not be under load during normal circumstances, as it mainly serve as a dampening system for the undulations produced in the track.

### 7.2.3. Test and Validation

#### **Static test**

Dampers used on LCM will be cyclically compressed during static test to analyze behavior of damper under load.

#### **Dynamic test**

A scaled down model of rail and LCM will be constructed to simulate actual test run, vibration profile and displacement will be recorded for future improvement.

## 7.3. VCM

The VCM was designed specifically to control the pitch and roll of the pod. The VCM is responsible to support the weight of the vehicle, and counter the effect of dive and squat due to overwhelming acceleration and deceleration of the vehicle, therefore a heavy load is to be expected. The propulsion unit have to keep a constant distance from the ground, and this requirement can only be achieved with a rigid suspension, therefore, in order to isolate vibration from said rigid suspension from the rest of the vehicle, the propulsion unit will be supporting its own weight, and linked to the rest of the vehicle via a pad of shock absorbing material.

### 7.3.1. Structural Design

The main VCM suspension are located at both ends of the vehicle to absorb most shock during acceleration and deceleration, and in case of emergency braking or defected rail. The design of choice is a robust system consisting of machined aluminium wheels and frame, with a safety factor of 15 during normal circumstance. According to simulation results, it is possible to remove some materials from the frame to reduce the weight, while maintaining a safety factor of 5, but this is not a priority because the weight reduction is not significant while more processing will be needed to manufacture these parts, and currently the weight of the suspension is not a limiting factor.

The main suspension of VCM is located at both ends of the vehicle and act directly to the ground, It consists of a suspension arm that transfer vertical displacement and shock from wheels to horizontally placed spring and damper that connects to the main frame of the vehicle.

Wheel and axle is a single latched piece to withstand extreme angular velocity, and is connected to the suspension arm with high speed roller bearings. Hinge between suspension arm and frame of the vehicle uses a durable bushing and shaft design to support load. The bearing and bushing of choice are designed to work in vacuum, and typically self-lubricated with graphite.

A small vertical suspension will act on the guiding rail for safety, and will not carry any load under normal circumstances. However in case of emergency braking these suspensions will become active and prevent the collision between the vehicle and guiding rail.

### 7.3.2. Stress Analysis

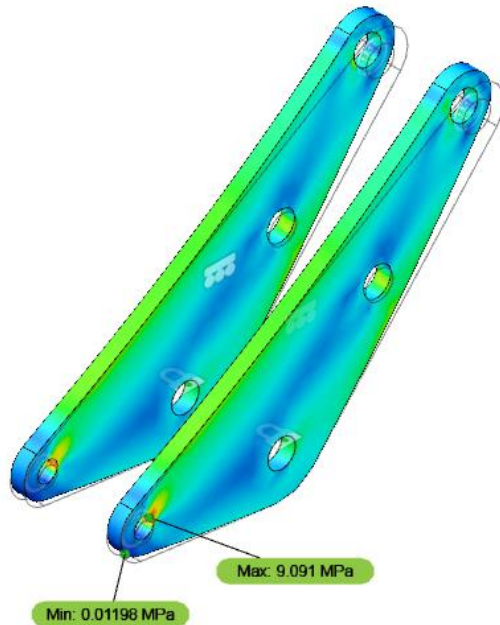


Figure 32, Maximum Stress 1

Maximum stress of 9.091 MPa occurs on bearing, which still have safety factor of 15

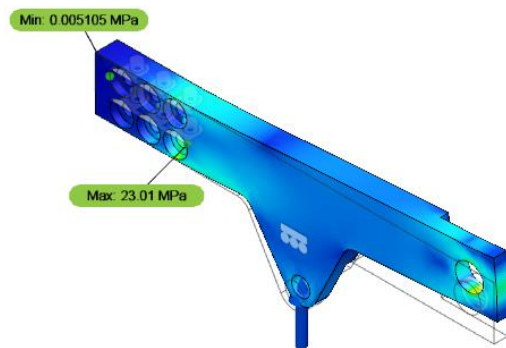


Figure 33, Maximum Stress 2

Maximum stress of 23.01 Mpa occurs on bolts, which have safety factor of 8

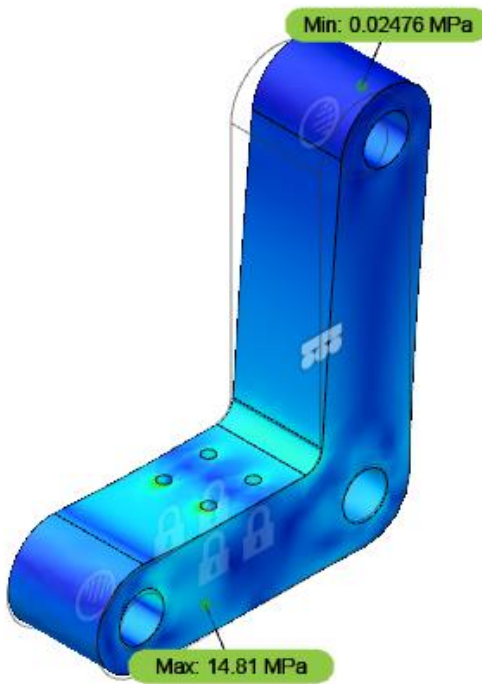


Figure 34, Maximum Stress 3

Max stress of 14.81 Mpa occurs on bolts, with safety factor of 10

### 7.3.3. Tests & Validation

Series of tests will be run on these suspension systems before launch to simulate and verify our design, and to make sure no design flaws will be passed to the final stage.

Test to be performed:

#### Static load test

The test will be performed to analyze the behavior of suspension due to static load. A hydraulic press will be used to simulate weight of the vehicle, and the equivalent effect of acceleration and deceleration. Displacement and deformation of test subject will be recorded, and adjustment will be made accordingly if any issues are observed.

#### Dynamic load test

The test will be performed to analyze the behavior of suspension due to dynamic load. A flywheel with a diameter of 4 feet will be accelerated to 2000 rpm to simulate the test track outer surface. The flywheel will be treated to have the same tolerance as the I-beam as given in the datasheet. When the test subject contacts with said flywheel, vibration and displacement will be recorded, and adjustment will be made accordingly if any issue is observed.

## 8. Structural

### 8.1. Overview

The structure encloses the various subsystems such as the Linear Induction Motor, Brakes, Stabilizer, Battery and Controller with the help of the frame. Moreover, it provides housing for a passenger cabin, and to protect components at low pressure since the passenger cabin will act as a pressurized chamber. The shell is also useful for reducing the air drag during high speed maneuvering, even though the pod is under lower pressure. It tends to increase the efficiency of the pod.

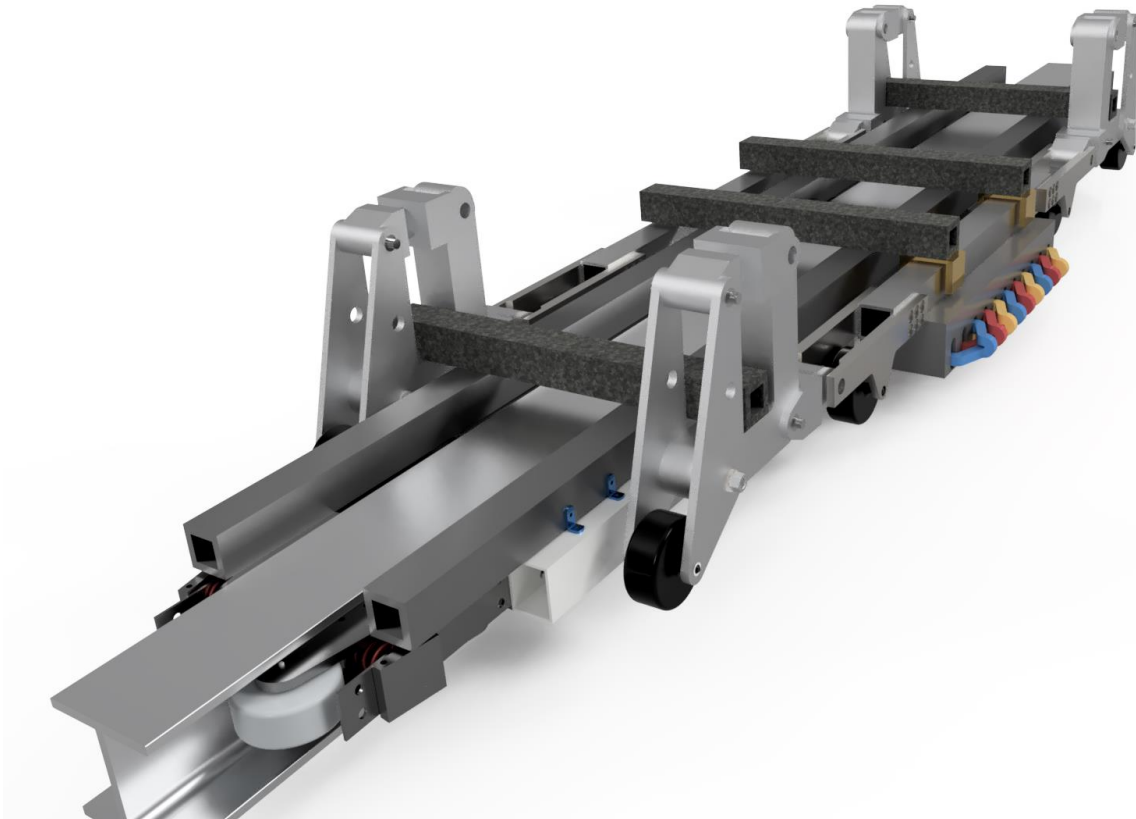


Figure 35, Frame

## 8.2. Shell

### 8.2.1. Overview

Even though the tube pressure is reduced to 0.1 atm it would still produce a slight drag coefficient when the pod reaches a speed of 500 kmph. Since our targeted speed of the pod is below Sonic (at this point in time), the Kantrowitz limit doesn't apply to our pod but, there will be the presence of drag force on the pod since tube isn't in an absolute vacuum. Aesthetics of the pod is a secondary purpose that the shell serves. The Shell is designed to protect the controls and sensors at high speed and increase efficiency of the pod.



Figure 36, Shell

### 8.2.2. Structural Design

The Shell is designed to encompass the entire frame, including all of its components. Taking aerodynamics into account even in a very low pressure space, the shell is efficient in its construction, and is made out of a lightweight Carbon-Fiber.

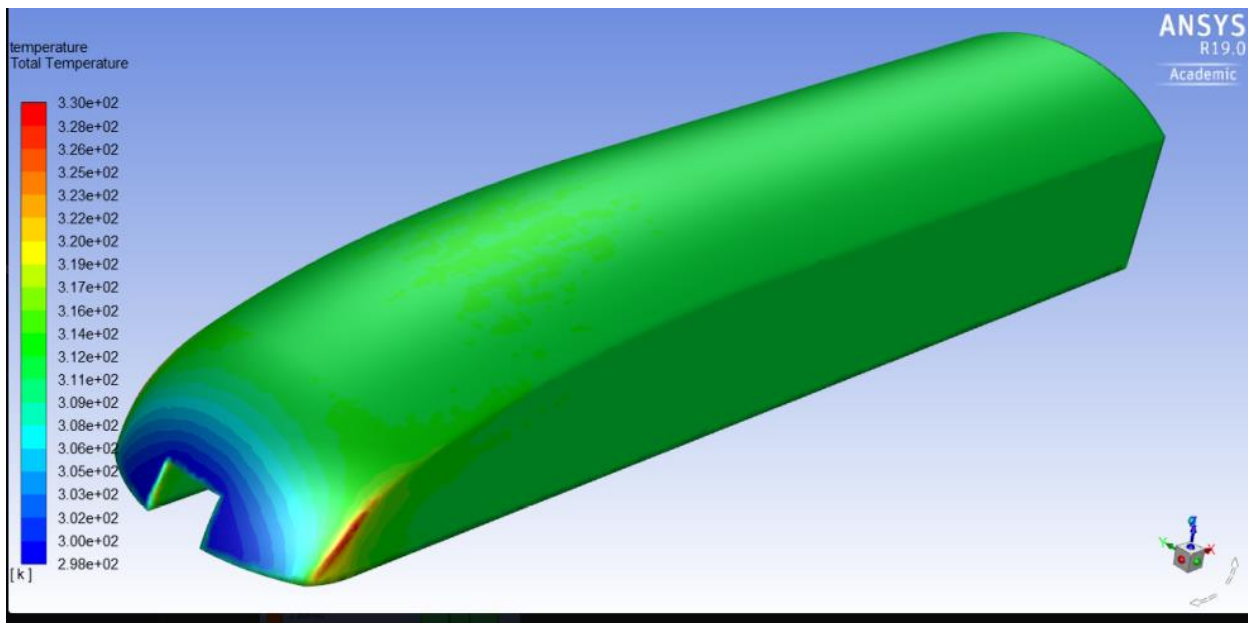
### 8.2.3. CFD Analysis

Boundary Condition	Description
<i>Velocity Inlet</i>	<b>500 km/h</b> <b>0.125 psi</b> <b>298 °K</b> Normal to face
<i>Pressure Outlet</i>	<b>0.125 psi</b> <b>298 °K</b>
<i>Inside Tunnel Walls</i>	<b>Smooth adiabatic walls</b> Slip condition (no shear stress)
<i>Shell</i>	<b>Smooth adiabatic walls</b> No-slip condition
<i>Rail &amp; Plates</i>	<b>Smooth adiabatic walls</b> Slip condition (no shear stress)

Table 6, Boundary Conditions

CFD Specifications	Description
<i>Solver</i>	Steady, Pressure Based
<i>Space</i>	3D
<i>Formulation</i>	Coupled
<i>Viscous Model</i>	Spalart-Allmaras
<i>Mesh</i>	1800000 Elements
$C_d$	1.58
$C_l$	0.046

Table 7, CFD Values



#### 8.2.4. Testing and Validation

A scaled prototype will be used in the University of Windsor's wind tunnel to estimate aerodynamic performance.

### 8.3. Frame

#### 8.3.1. Structural Design Cases

The following figure represents the case loading in which the weight of the components are connected to the pod. The weight of the components are the only forces acting on the frame.

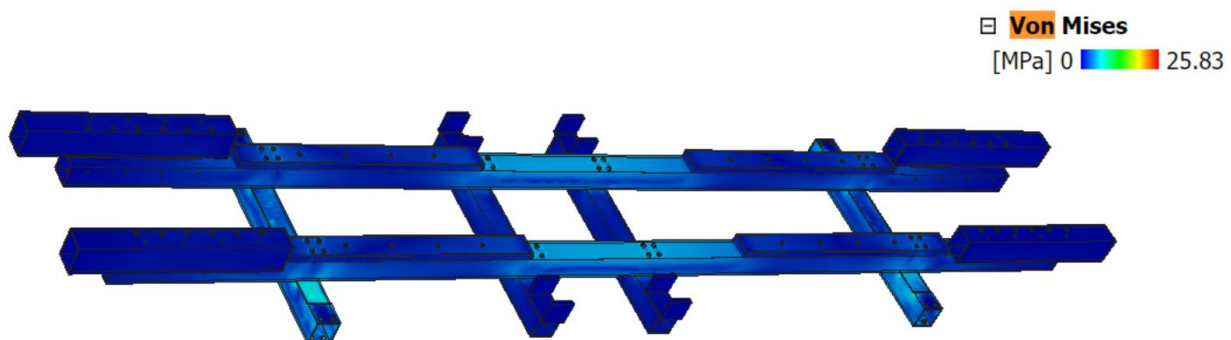


Figure 37, Frame Static Loading

### 8.3.1.1. Initial Acceleration Case

The following figure represents the stress that the frame experiences when the pod is accelerating forward. The pod is designed to go from 0 m/s to 140 m/s in a time interval of around 7.2 seconds.

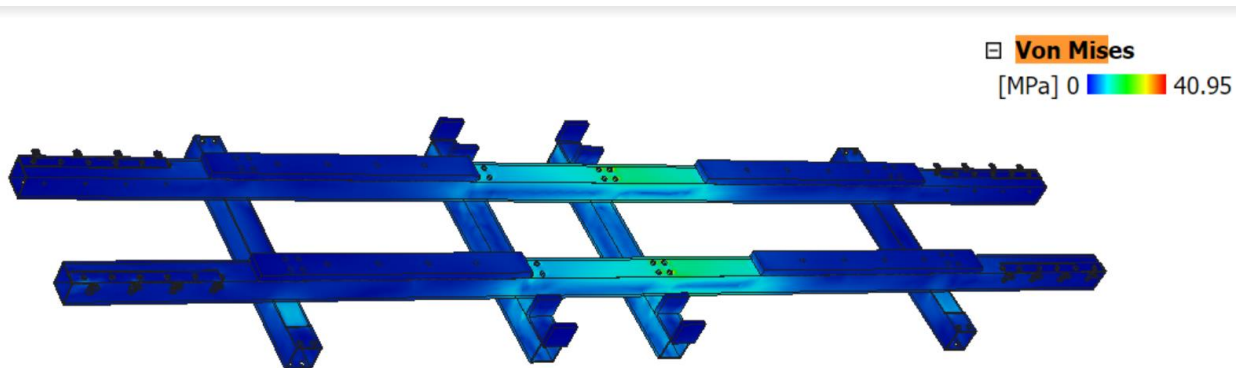


Figure 38, Frame Accelerative Loading

### 8.3.1.2. Nominal Deceleration

The following image represents the stress that the frame is under when decelerating. During decelerating the LIM ceases its function and the friction brakes are activated. The frame is under the most stress under these conditions and the minimum safety factor was simulated to be 4.2.

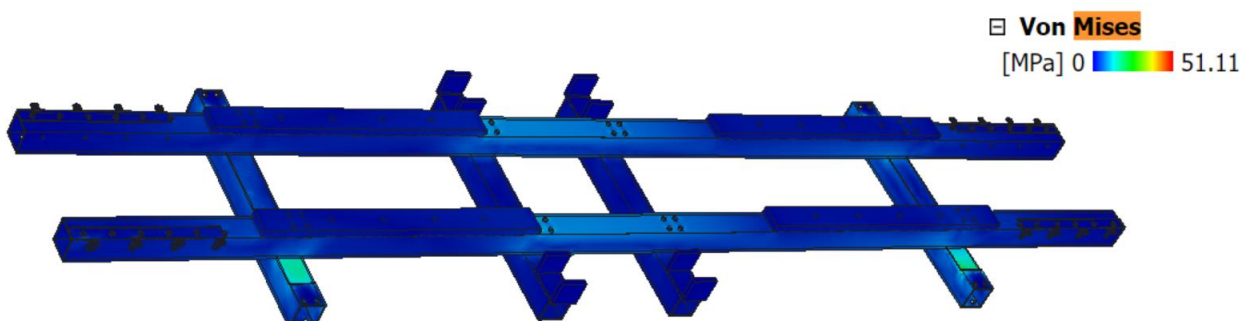


Figure 39, Frame Decelerative Loading

### 8.3.1.3. Reasonably Foreseeable Off-Nominal Crash

Although the current suspension system is specifically designed to be durable and reliable, an unforeseen incident may still occur. In case the stabilization and braking system fails, the frame should be able to retain its structural integrity, meanwhile absorbing enough energy to protect passengers and equipment.

The main frame is made from steel square tubes and is bolted together with steel brackets as reinforcements. This frame design is focused on strength and weight carrying ability, and can achieve a safety factor of 8.33 under static load. The front portion of the frame and shell will have aluminum mesh inside, and act as a bumper to absorb energy during impact.

### 8.3.1.4. Thermal Analysis

The vehicle frame and pressure vessel are all made from stainless steel and aluminum, and they can both act as a heat sink. Given the heat generated by the battery and the motor is negligible, the thermal stresses inside the frame are also negligible.

### 8.3.1.5. Testing and Validation

Static load test:-

The test will be performed to analyze the behavior of the frame structure due to a static load. A hydraulic press will be used to simulate loads, and an equivalent effect of acceleration and deceleration. Displacement and deformation of test subject will be recorded, and adjustment will be made accordingly if any issue is observed

## 9. Power

### 9.1. Overview

The power system aims to provide safe, reliable power to the entire pod and each of its subsystems. It converts HV DC power to 3 phase AC power which is essential to the operation of the LIM and the movement of the pod. This system consists of a HV battery pack, two 24V battery packs, battery management systems (BMS), an inverter, multiple safety mechanisms and lots of wires.. High voltage power is provided to the LIM and low voltage power is provided to all other components.

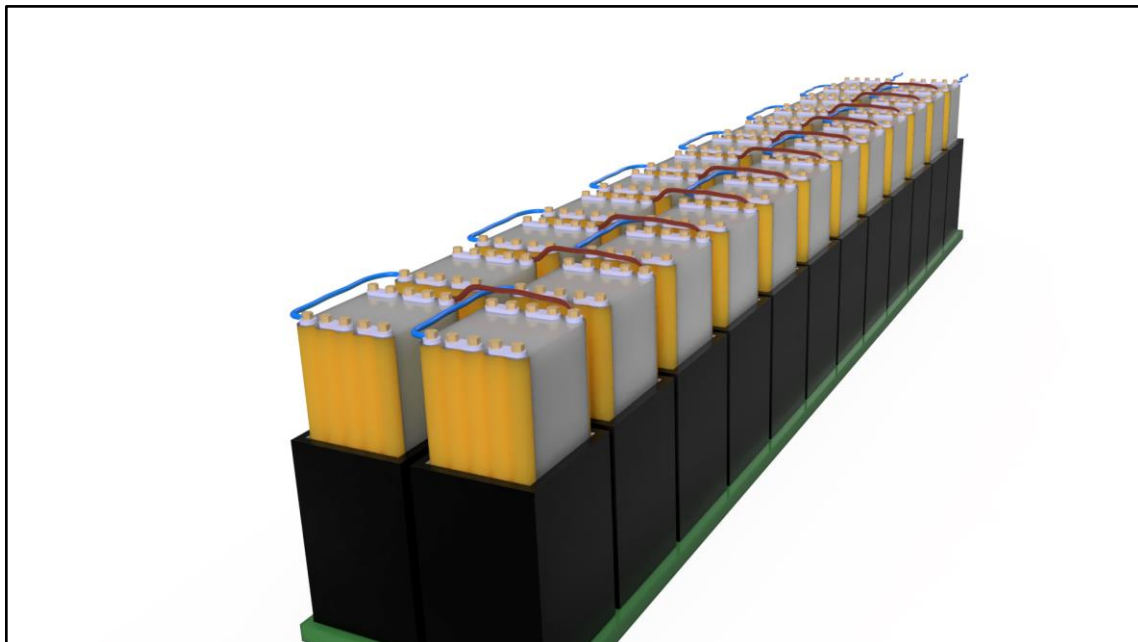


Figure 40, HV Battery Pack

## 9.2. Battery

### 9.2.1. Design

#### 9.2.1.1. High Voltage Battery Pack



Figure 41, Battery Cell

The HV Battery will be constructed using LiNiMnCo cells of prismatic/pouch type due to their high energy density compared to other types of batteries. Each cell is 3.7V and has a capacity of 10Ah. To create our battery of desired voltage, 120 battery cells will be connected in series forming a 120s1p configuration calculated as below:

Number of cells in series:

$$\frac{\text{Battery pack voltage (444V)}}{\text{Cell voltage (3.7V)}} = 120 \text{ cells}$$

Number of cells in parallel:

$$\frac{\text{Battery capacity (7.5Ah)}}{\text{Cell capacity (10Ah)}} = \sim 1 \text{ cell}$$

Total number of cells:

$$\text{Number of cells in series (120)} \times \text{Number of cells in parallel(1)} = 120 \text{ cells}$$

Expected overall weight of HV battery pack:

$$\text{Weight of each cell (200g)} \times \text{Total number of cells (120)} = 24\text{kgs}$$

Typical LiNiMnCo battery cell dimensions are 162 X 60 X 11 mm<sup>3</sup> (L x B x H) and specifications are as shown below from the suppliers' battery specifications sheet:

Item	Specifications		Remark
Typical Capacity	10000mAh $\pm$ 5%		25°C, 0.2C <sub>5</sub> A discharge
Nominal Voltage	3.7V		25°C, Average Voltage at 0.2C <sub>5</sub> A discharge
Charge Current	Standard: 0.2 C <sub>5</sub> A; Max: 1C <sub>5</sub> A		Working temperature: 0~45°C
Charge cut-off Voltage	4.20 $\pm$ 0.05V		
Discharge Current	Continuously:4C <sub>5</sub> A; Max: 10C <sub>5</sub> A		Working temperature: 0~60°C
Discharge cut-off Voltage	2.75V		
Cell Voltage	3.76~3.90V		When leave factory
Impedance	$\leq$ 5mΩ		25°C, AC 1KHz after 50% charge
Weight	Approx: 200g		
Storage temperature	$\leq$ 1month	-10~45°C	Best 20 $\pm$ 5°C for long-time storage
	$\leq$ 3month	0~30°C	
	$\leq$ 6month	20 $\pm$ 5°C	
Storage humidity	65 $\pm$ 20% RH		

Table 8, Battery Specifications

### Modules

The 120cell HV battery will be separated into 24 smaller modules. Each module will consist of 5 cells in series (5s1p). Smaller modules will allow for easier construction, maintenance and handling of the cells and battery pack. Each module will have 3 cables coming out of it: a positive terminal wire, a negative terminal wire, and the BMS wiring harness. The modules will be connected together in series to obtain the final voltage.

To efficiently monitor the cells of the battery in series, a BMS board is installed between the terminals of each cell during battery construction. These boards are The BMS master communicates the health of the cell through a communication harness attached to these BMS boards.

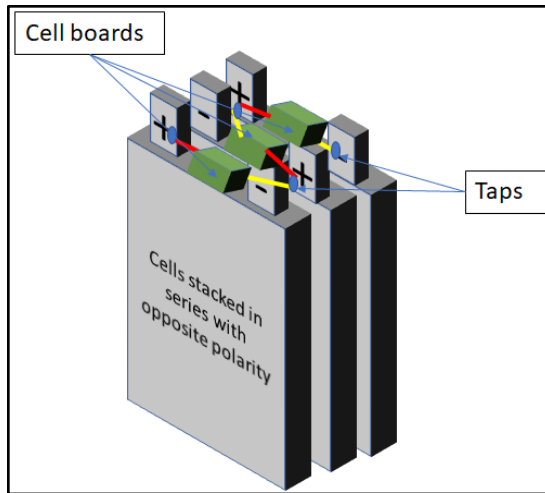


Figure 42, Cell Structure

- Battery health, status, and diagnostics will be determined with the help of the following parameters determined using sensor circuits and BMS:
  - Battery state of charge (SOC): SOC is battery charge status at any given time and is equivalent to fuel level sensor in diesel or gasoline engines. Since, battery charge status cannot be determined directly with the sensor, it will be modelled using simple OCV-R model.
  - Battery cell voltage and temperature measurements: These values will be sensed by the cell board mounted on each cell and connected to positive and negative terminals of each cell. Cell board then sends information to the BMS.
  - Battery voltage and current: Pack voltage and current will be reported by pack voltage and current sensed by the circuit boards mounted on the battery pack and communicated to BMS.
  - Cell Balancing: Cell balancing will be employed in BMS and will play a vital role in optimizing the battery capacity. Cell balancing is discussed in detail in BMS functions.

- Battery Thermal management:

Heat dissipated from a battery is divided into three main parts:

1. Internal resistance of battery cell
2. Entropy change in battery cell component during battery discharge
3. Convective heat transfer in ambient conditions.

Since, heat generated due to internal resistance is major contributor, heat generated from the battery will be calculated based on following equation and simple model:

$$m * C_{cell} * dT_{cell} = I^2 * R$$

Where,

- $m$  = mass of one battery cell(kg)
- $C_{cell}$  = Specific heat of cell (J/kgK)
- $dT_{cell}$  = Rise in cell temperature(K)
- $I$  = current drawn from battery cell (A)
- $R$  = internal resistance of battery cell (ohm)

The model parameters used are as below:

- $m = 200\text{g}$
- $I = 100\text{A}$  (Assuming max permitted discharge current rate at  $10C_5\text{A}$ ) during discharge  
=  $10\text{A}$  (Assuming max permitted charge current at  $1C_5\text{A}$ ) during charge
- $R$  = internal cell resistance ( $0.02\Omega$ )
- $T_{cell}$  = max operation cell temperature
- $T_{amb}$  = ambient temperature ( $25^\circ\text{C} \rightarrow$  Expected tube temperature)

Considering above parameters, the expected temperature rise (<5 degrees) during discharge is not too high, hence currently no cooling system for high voltage battery pack is employed.

- Battery Charging:

Battery charging system will consist of a level 1 EVSE (Electric vehicle supply equipment) compatible with 120V/230V AC power sources. An onboard charger to convert low voltage AC to high voltage DC power. An exemplary picture of a level 1 charger with SAE J1772 male and female connector is shown in the figures below.



Figure 43, Battery Charger



Figure 44, Charging Port

- Further steps:

With the current battery design, the pod is expected to reach a speed of 16m/s. In order to meet the target speed of 139m/s, the battery will be scaled to 600 kW DC power with an estimated 120s7p connections and will be arranged in different modules to fit it onto the pod using the same calculations as above.

The 120s7p connection is expected to be arranged in 10 modules with 12s1p connection in each module and will weigh approximately 168 kg. However, a series of simulations, iterations and calculations combining LIM and battery systems will be conducted to arrive at a suitable weight and size of the battery system and achieve the speed target.

Also, the high power rating will lead to more heat generation and hence a suitable cooling system will be employed based on maximum cell temperature values achieved based on the selected model.

### 9.2.2. (25.9)V DC battery

26V DC battery is power source to all 3.3V, 5V, 12V and 24V electrical loads on the pod such as sensors, BMS, braking, lightings (if any) and other ancillaries except for linear induction motor. Battery voltage of 26V battery will also be monitored by BMS to ensure proper supply power supply to all the major electrical loads.

LiNiMnCo battery cells similar to the ones used for high voltage battery pack will be arranged in series and parallel configuration to form a 26V battery system. It will essentially be 7s1p configuration. There will be another exact same system of 26V with same configuration, which will be used as a backup in case of failure of first system. The controls to switch from one battery pack to another will be done with the help of BMS.

Parameter	Specification
Battery cell	LiNiMnCo (Lithium ion - NMC type)
Battery pack voltage	26V (each)
Battery capacity	10Ah

Table 9, 26V Specs

Certain sensors employed in pod require an input voltage of 12V, 5V and 3.3V. DC-DC Buck Converters will be used to step down 24V to provide 12V, 5V and 3.3V power to all the sensors. Although the concept of a voltage divider is simply applicable and cheaper, it is not very efficient in reserving power since the input voltage is reduced by dissipating power through the resistors in the form of heat. Buck converters on the other hand, are very efficient at reserving power and in fact help step up the output current. This is done so by the use of switches(transistors and diodes) and energy storing elements(inductor and/or capacitor). The details of the buck converters being used are given below:

Parameter	Specification
Manufacturer	DROK

Input Voltage	6V-65V
Output Voltage	0V-60V
Output Current	0A-8A
Model Number	200220
Dimensions	104x59x46 mm

### 9.2.3. Battery safety:

Battery is a critical component for safe operation of the pod and hence it becomes imperative to employ safety methods to meet this requirement. Different safety components and strategies are used at different levels of battery subsystem starting from cell to module and to pack.

**Insulation:** Battery modules will be separated by an insulation to provide thermal and electrical isolation.

**Software protection:** BMS continuously monitors critical parameters of voltage, current and temperature of the battery module and pack. It also monitors voltage and temperature of each cell in a module. Any short circuit or low/high voltage scenario will be detected by BMS in order to safeguard battery system and hence the pod. It will also disconnect the charging circuit in case of overcharging.

**Battery pack fuse:** To protect battery pack in case of any external and internal short circuits. 20A battery pack fuse is considered to protect 15A of battery considering below equation:

$$\text{Fuse rating} = (\text{Current} \times 1.25) \text{ amps}$$

**Circuit Interrupted Device (CID):** Each battery cell will be equipped with CID to prevent overcurrent cases in a cell by opening the connections between positive pole and negative pole of the cell.

**Positive Temperature Coefficient (PTC) elements:** PTC element within each battery cell protects it from overheating and limits external current in case of external short circuits.

## 9.3. BMS

### 9.3.1. Design

To monitor both the HV battery and 24V battery, an Elithion Lithiumate BMS will be implemented. Elithion has a good reputation when it comes to providing BMS solutions for many different projects and student design teams as well as vehicle designers. They require minimal wire connections which allow a cleaner, simpler layout. This BMS will be able to monitor the voltage and current as well as the temperature of each cell. The BMS is able to communicate its information using a CAN bus and therefore will allow for easy data transfer between the BMS and the microcontrollers.

A student made custom BMS was considered. However, the large quantity of cells in addition to cells in series proved to be too complex to design. The design would not be as efficient as industry-made ones and the safety mechanisms would not be as extensive, resulting in a less reliable BMS.

The BMS controls the main HV contactor, enabling or disabling HV power to flow into the system, thus connecting or disconnecting it.

### 9.3.2. SOC

The state of charge of the battery will be controlled and monitored by the BMS. The BMS is able to monitor the voltage level of each cell and as a result, will provide the microcontrollers with information on whether or not the battery needs to be charged.

### 9.3.3. Cell balancing

When a battery is composed of many cells, it is highly unlikely that all cells will have the same capacity. This means that some cells might become empty before others when discharging and some cells will reach maximum capacity before others when charging. This needs to be accounted for in order to prevent over charging and discharging of the cells because it could damage them. As mentioned before, the BMS is able to monitor the voltage level of each cell and therefore will be able to notify the microcontrollers that a cell has reached its lowest voltage, i.e indicating that the SOC is low, and will also do the same when a cell has reached its highest voltage, i.e indicating that the SOC is high. This BMS can balance the voltage of cells while in charge, allowing each cell in the battery to have equal voltage.

### 9.3.4. Controls BMS

There is a 24V 20A 7S BMS for each 26 V battery. If the BMS of the main 26v battery faults, the circuit will switch to the backup BMS and 26V battery and that will then supply the pod's low voltage power.

## 9.4. Inverter

### 9.4.1. Overview

The inverter system converts the 444VDC power from the battery into 400VAC 3 phase power for the Propulsion System. The output of the inverter will be connected as input to a variable frequency drive. The output voltage and frequency of 400 Hz will be inputs to the LIM. This will directly influences the acceleration and direction of the pod's speed. DC power is connected to the inputs of the IGBTs. The block diagram below describes the different section of the inverter system. The red lines represent the voltage while the green block represent the LV section.

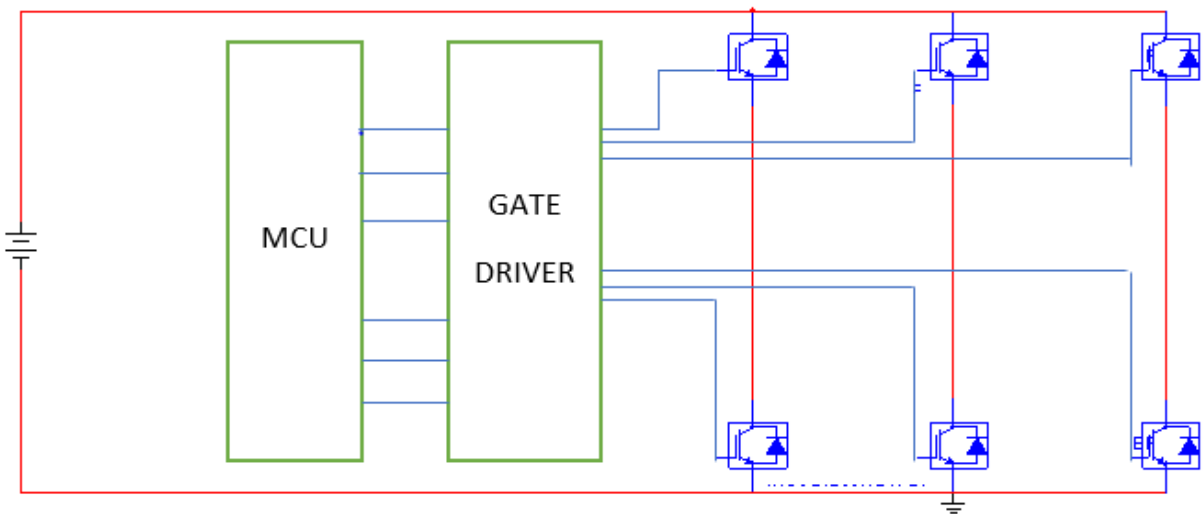


Figure 45, Invertor Diagram

### 9.4.2. Design

#### 9.4.2.1. Gate Driver

The gate driver is the device that ultimately controls the gate driver has 6 output terminals which will provide the drive current to an IGBT gate to switch the current ON or OFF to vary the current flow. The IGBT will switch ON to provide high current to drive the load. The driver is also an optocoupler. It optically isolates the low voltage control circuitry from the high voltage load (LIM). The optocoupler protects the sensitive electronics and the user from voltage spikes, RFI, noise and EMI. It acts like a brick wall and also allow clean signals to pass through. The gate drivers provide a high voltage output from 15 to 32 V to turn on the IGBT and a negative voltage to turn off the IGBT.

Inside the gate driver, the LED activates a photo transistor that will activate a half-bridge transistor to an ON state. This transistor sends a high positive voltage to the IGBT. Whenever the LED is turned off, a second transistor is turned ON thereby sending a negative voltage to discharge the gate capacitor of the IGBT. This leads to the emitter terminal shutting out.

Usually, a switching signal to an IGBT is generated by a microcontroller, which is limited to a few milli-amperes of current. An IGBT that is driven directly by such a logic circuit would switch very slowly. During switching, the gate capacitor of the transistor may draw current so quickly that it causes a current overdraw in the logic circuit or microcontroller, causing overheating which leads to permanent damage or even complete destruction of the chip. This is a design and safety issue. In order to prevent this, a gate driver is put between a microcontroller and the IGBTs. Gate drivers have higher drive current than microcontroller.

The ADuM4223 will be the gate driver used to drive the IGBTs. It is a 4 amp isolated, half-bridge gate driver designed by the Analog Devices, Inc., iCoupler® technology. It operates with an input supply ranging from 3.0 V to 5.5 V, providing compatibility with lower voltage systems. ADuM4223 offer the benefit of true, galvanic isolation between the input and each output. Each output may be continuously operated up to 537 V peak relative to the input, thereby supporting low-side switching to negative voltages. The differential voltage between the high-side and low-side may be as high as 800 V peak. As a result, the ADuM4223 provides reliable control over the switching characteristics of IGBT configurations over a wide range of positive or negative switching voltages.

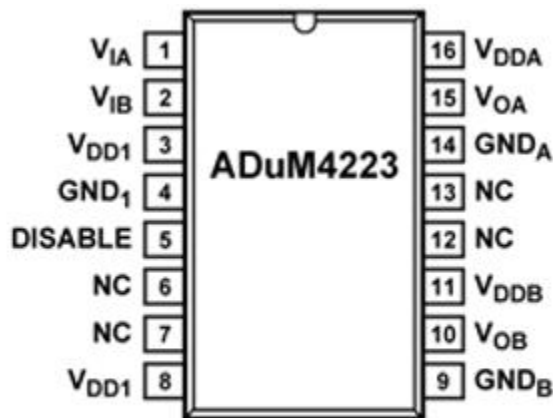


Figure 46, ADU IC

#### 9.4.2.2. Switches (IGBT)

IGBT stands for Insulated Gate Bipolar Transistor. An IGBT is a voltage-controlled device that is used as a switching element in power supply circuits and motor drives. IGBT has 3 terminals: The gate which is the electrically isolated control terminal for each device, the other terminals are called the collector and emitter. To operate IGBT, typically a voltage has to be applied to the gate that is relative to the emitter of the device. Varying this gate voltage will vary the drain

current of the IGBT. Dedicated drivers (gate drivers) are used to apply voltage and provide drive current to the gate of the power device.

Each switch will consist of 6 IGBTs, with 2 switches for each phase, one connecting the positive DC terminal to phase output and the other connecting phase output to the negative DC terminal. The LIM will be driven by the IGBT module.

#### 9.4.2.3. Microcontroller

Arduino Uno will be the logic brain of the inverter control system. It was chosen due to its robustness, capability of being programmed in C language, configurable digital pins, and the capability to communicate with other arduinos and raspberry pi used in other subsystems.

The Microcontroller has 14 digital pins, which can be programmed as either input or output pins. They operate at 5v which is required voltage of the gate driver.

#### 9.4.2.4. Safety

1. The gate driver protects the MCU from voltage spikes by acting as a shield
2. When there is abnormal voltage, the MCU deactivates the inverter by stopping voltage signal to the gate driver

### 9.5. Failsafes

#### 9.5.1. Battery

Battery pack will be protected with different protecting devices discussed in battery safety sections and listed below:

1. Software protection via BMS
2. Circuit Interrupted Devices (CIDs)
3. Battery pack fuse
4. PTC elements

In addition, in case of 26V battery system failure there is another backup battery of 26V and both will be controlled by BMS.

### 9.6. Pressure Vessel

#### 9.6.1. Pressure Vessel for High Voltage Battery

Batteries, BMS and the inverter along with sensors needs to be kept in the pressure vessel due to the pressure inside of the tube. Internal pressure of the pressure vessel is 14.8 psi, whereas external pressure of the tube is 0.15psi. Since pressure vessel is being manufactured by the uWinLoop team, it is designed with consideration to ensure that vessel has a factor of safety of

at least 3. The pressure vessel has a rectangular cross section with enforced members installed inside and outside.

The thickness of the main body is 5mm and is made out of aluminium T6-6061. Solid horizontal members are installed on the outside of vessel to increase structural integrity of the vessel. Internally three sides of the vessel are reinforced with ribs around the inner perimeter, spaced equally along the length of the vessel. Maximum dimensions of the pressure vessel for LIM battery pack are 1354 x 264 x 284 mm, with a mass of 43 kg. The vessel has a factor of safety of 4.62 based off of the maximum stress in the ANSYS simulation. The vessel will be inspected thoroughly after being manufactured to ensure quality. The vessel will also be pressure tested for 1.5 times the max operating pressure. Hermetic connectors will be installed on the side of the vessel to allow electronic communication and power transfer between the inside and outside of the vessel.

There will be 2 different connectors installed on the vessel. One will be a 2 pin, High-Voltage connector for power transfer and the other will be a 16 pin connector for the BMS-MEB communication.

### 9.6.2. Pressure Vessel for Control Battery and Controls

The smaller battery pack is kept in a separate pressure vessel to ensure the safety of each battery and in case either of the battery packs or pressure vessels is compromised. The pressure vessel for the smaller battery pack has a design that is similar to that of the large pressure vessel, with maximum dimensions of 484 x 244 x 284 mm, with a mass of 17 kg. The vessel has a factor of safety of 4.91 based off the maximum stress in the ANSYS simulation. The vessel will be inspected thoroughly after being manufactured to ensure quality. The vessel will also be pressure tested for 1.5 times the max operating pressure.

The vessels are being designed to have a two fault tolerance. This is the ability to sustain operation after a failure has occurred, where the failure can be of mechanical, electrical, or programmable origin. To achieve this goal, the vessel is designed so that during a subsystem failure, the vessel as a whole is still capable of completing its task, or at the very least, safely release its pressure. Design for fault tolerance also motivates a modular system of two separate pressure vessels, with each module performing specific tasks while communicating with other modules via controller. Both pressure vessels in the current configuration are manufactured from 6061-T6 aluminum alloy that is hard-anodized for electrical insulation and corrosion resistance.

This vessel will have 2 hermetic connectors installed on the vessel, one for CAN connections and one for 24V, 12V, 5V, 3.3V supply lines.

### 9.6.3. Safety features

- A Barometer sensor module is installed inside each pressure vessel to monitor the slightest change in the internal pressure. Its primary function is to monitor internal pressure so that in case of an emergency/failure controls can release the check valve to release pressure inside the vessel.
- Power regulating and battery monitoring circuitry is included inside each battery pressure vessel to protect against low voltage and over current situations.
- Operation pressure of above designed vessel is 14.7psig (or 0.1psi) which is below the allowed limit to use various connectors.
- Each vessel has a factor of safety of at least 4.6
- Each vessel will be equipped with; an electronic release/regulator valve with a 0.25-0.05s response time, a mechanical check valve and a manual release valve

### 9.6.4. Pressure Vessel FEA Analysis

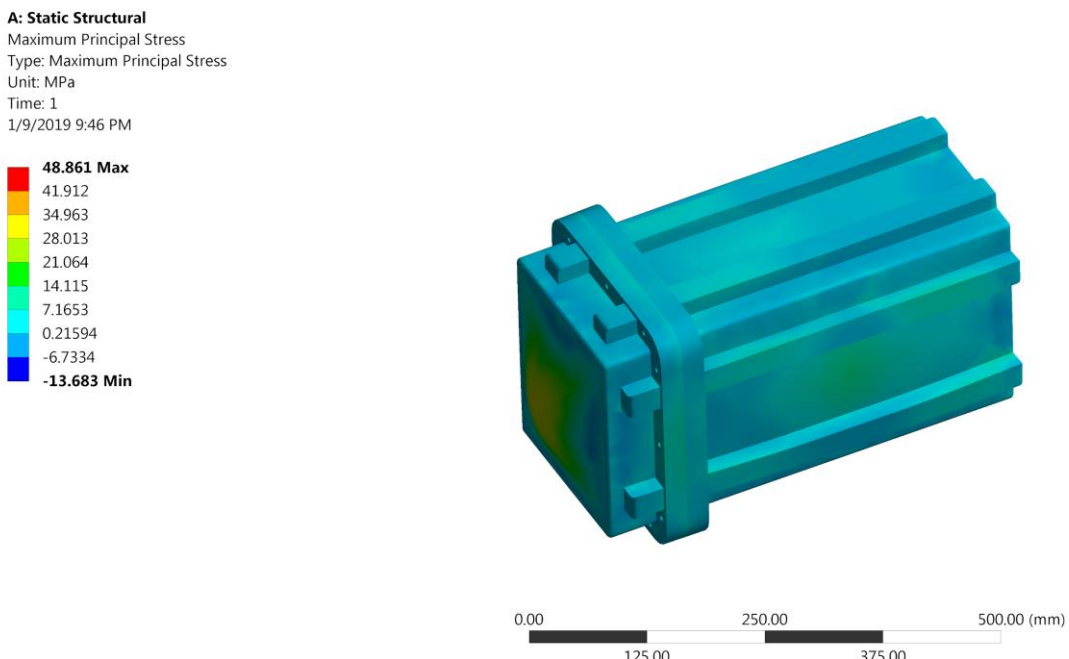
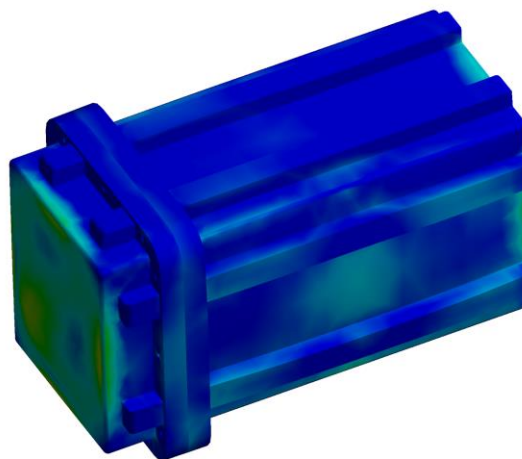
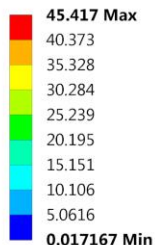


Figure 47, Maximum Principal Stress of Small Vessel

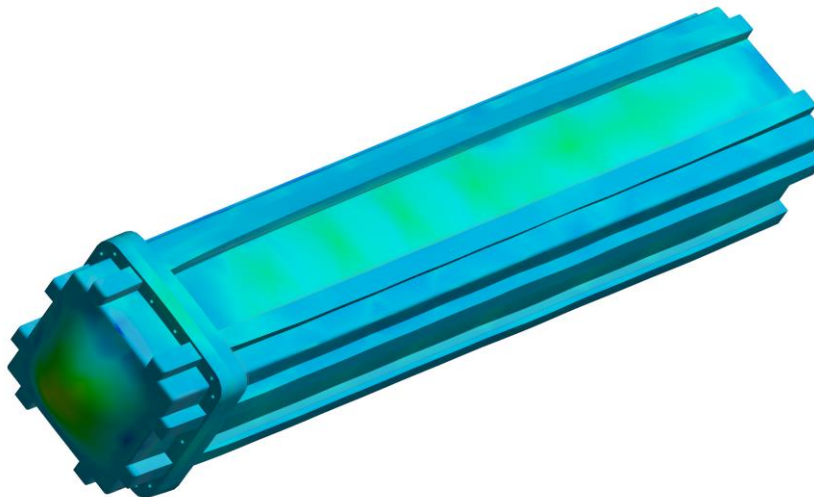
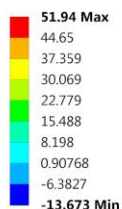
**A: Static Structural**  
 Equivalent Stress  
 Type: Equivalent (von-Mises) Stress  
 Unit: MPa  
 Time: 1  
 1/9/2019 9:45 PM



0.00      250.00      500.00 (mm)  
 125.00      375.00

Figure 48, Equivalent (Von-Misses) Stress of Small Vessel

**A: Static Structural**  
 Maximum Principal Stress  
 Type: Maximum Principal Stress  
 Unit: MPa  
 Time: 1  
 1/9/2019 9:03 PM



0.00      300.00      600.00 (mm)  
 150.00      450.00

Figure 49, Maximum Principal Stress of Large Vessel

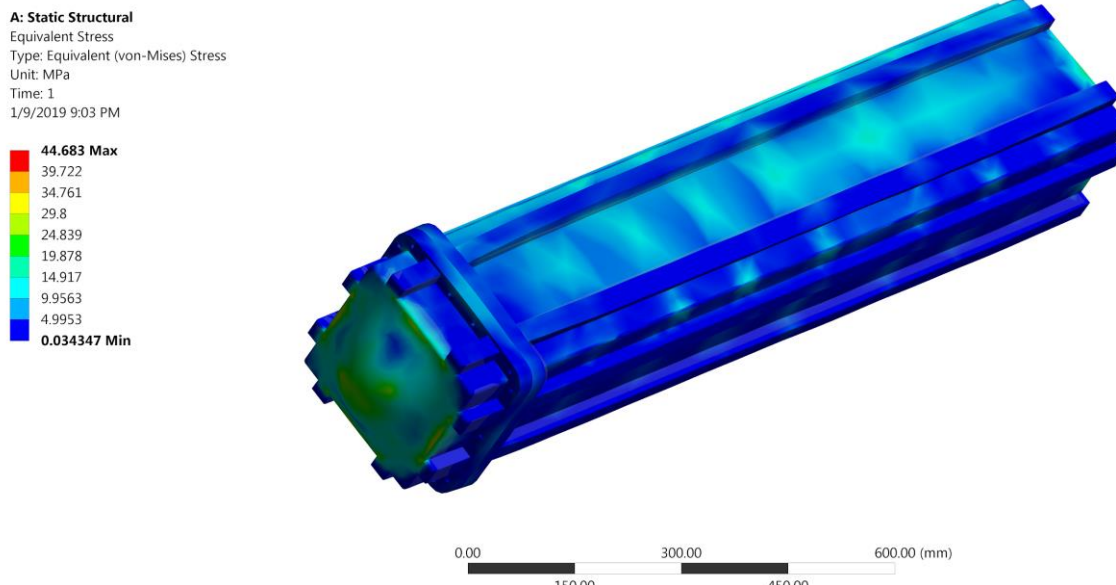


Figure 50, Equivalent (Von-Misses) Stress of Large Vessel

## 9.7. Testing

### 9.7.1. Battery

#### 9.7.1.1. Battery Cell Testing:

LiNiMnCo battery cell will be tested at standard discharge current of 4C<sub>5</sub>A starting from a minimum possible pressure to 1 atm pressure for an expected duration of run, to ensure no arcing during all possible operation conditions of the pod, as per the competition requirement.

#### 9.7.1.2. Battery Pack Testing:

Similar to battery cell, battery pack will also be tested as per the competition requirement from minimum possible pressure to 1 atm pressure.

#### 9.7.1.3. Pressure leakage testing

Due to the lack of access to vacuum chambers, a simple approach was taken to test the leaking. The pressure vessel will be pumped with 1.5 times the working pressure and the pressure drop over time will be measured to determine whether or not the vessel is leaking.

### 9.7.2. BMS

In order to test the BMS, an HIL (hardware-in-loop) testing will be implemented. Essentially, an emulation using sensors and actuators acts as a interface between a simulation of the pod and the embedded system. Since this emulation mimics the load of the actual pod, it will draw current and power that is very similar, if not exact, to the real thing. Keeping in mind that this is all based on a simulation, this allows for direct access to the battery itself which would otherwise be placed in a prototype. The battery is then available to be measured with measurement tools such as a multimeter, and those results can then be compared to the results of the BMS to see if the BMS is working as intended. It is important to note that if the BMS is not providing correct results, it could be that the BMS is not working or one of the cells is not functioning properly. A simple way to test this is to compare the rate of charge of the cells. First ensure that there is minimal discrepancies between the cell voltages (maximum 0.1V) and then allow the battery to charge. After a set time, check to see if some cells charged more quickly than others i.e check to see if the discrepancies increased. If they did, then it is possible that the cells that did not charge quickly enough are dead or close being dead in which case it was a problem with the cells. However if the cells charged at the same rate, then the BMS must be further inspected to fix the problem.

### 9.7.3. Inverter

The simulation was done with Simulink. Inverter system is an open-loop controlled IGBT based inverter. It consists of 6 IGBTs; 2 IGBTs are connected in series per phase. The input of each IGBT is connected to 400 VDC and the output is connected to a 3 phase load. Pulse voltages are used to switch-on the IGBTs. The IGBTs are arranged at different phase angles to achieve 3 phase AC voltage.

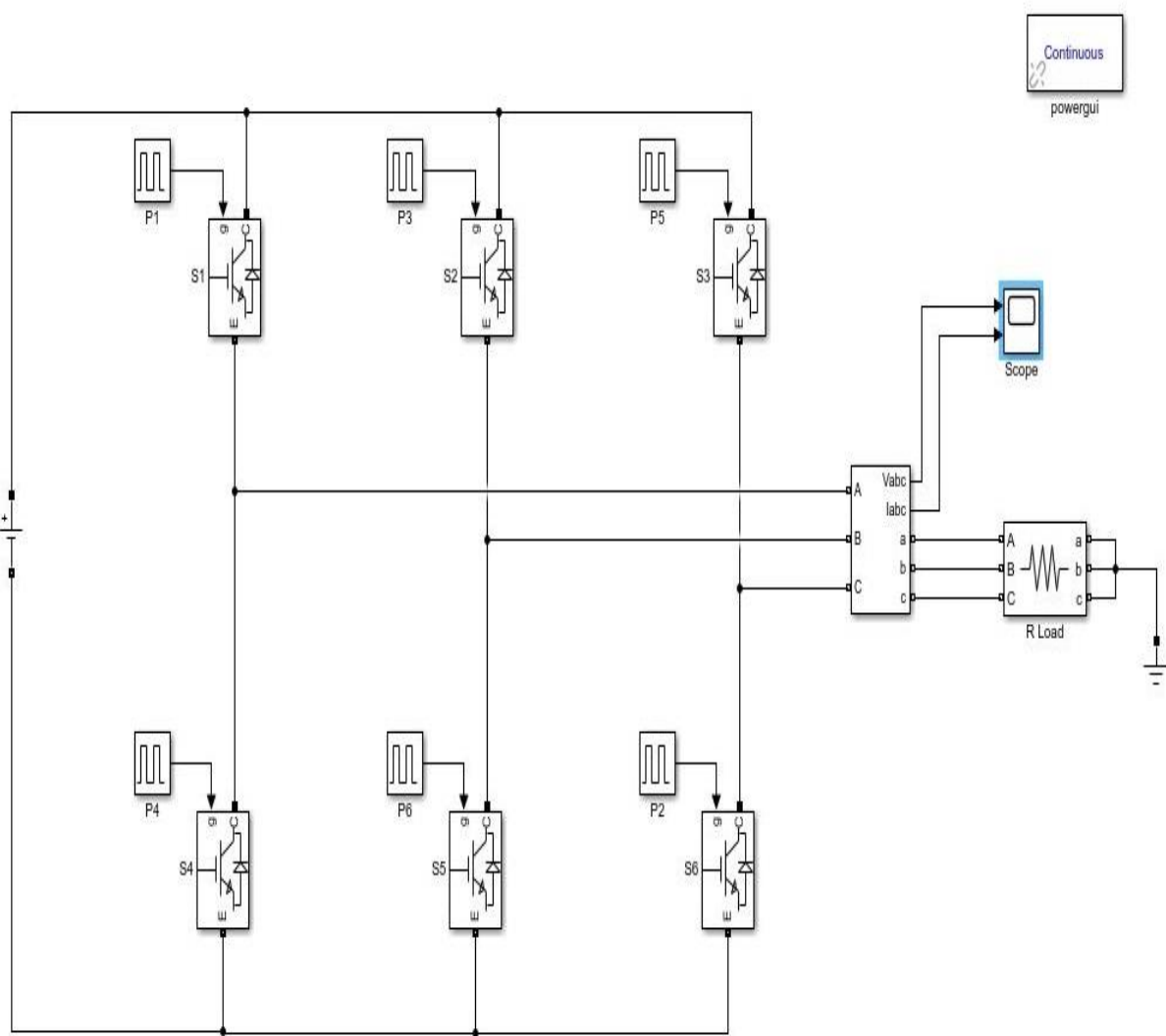


Figure 51, Simulink Model

The image below is the simulation performed of the circuit. This waveform is of Voltage vs Time. The simulation time was reduced from 0.5sec to 0.03 sec in order to increase the clarity of the plot. The sinusoidal wave has an amplitude of 400

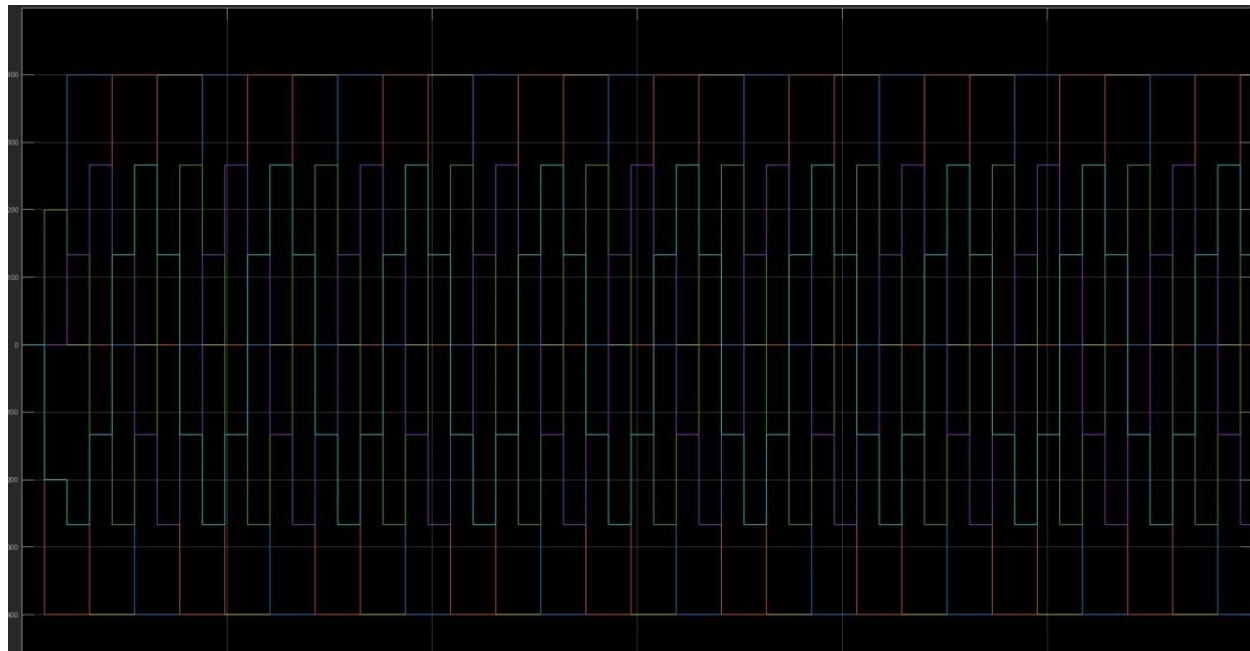


Figure 52, Waveform

## 9.8. Failure Modes

Failure	Description	Result
Battery	HV battery fails	BMS will trigger message to MEB to disconnect LIM and inverter as well as engage breaks
Battery	Main 26V battery fails	BMS switches to back up Battery
Battery	Back-up 26V battery fails	Main contactor to the HV battery will disconnect and shut down and brakes will deploy.
Inverter	Loss of inverter	MEB will disconnect HV power to the inverter, shut down the inverter and engage breaks
BMS	Loss of power to BMS	Loss of BMS will open main contactors to HV battery

## 10. Embedded

### 10.1. Introduction

The Embedded system of the pod serves as the link between the software control system and the hardware of the other systems of the pod. The main goals in the development of the embedded control system were: redundancy and modularity. This was achieved with the use of two Main Embedded Boards that act as the central controller which are connected to the Sensor and Controls hubs via the CAN.

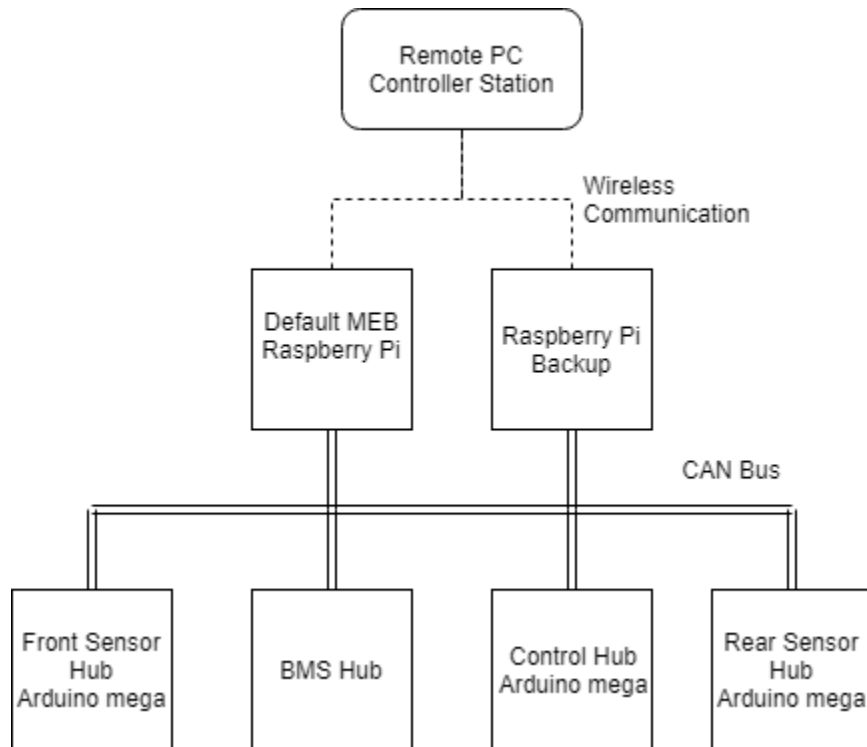


Figure 53, Control Diagram

### 10.2. Main Embedded Board (MEB)

The purpose of the main embedded board is to allow for the control of the pod, the board is used to get sensor data from the sensor hubs and send control data to the control hubs. The MEB will also receive data and interface with the BMS, a separate controller used to control the battery and power system. The two MEBs will be via the main CAN bus that will be used to link all of the hubs on the pod. The Main Embedded Board will consist of a Raspberry Pi with a shield to allow for CAN communication. The boards will also be used to send and receive the network data to the radio to allow for telemetry and remote control.

### 10.3. Sensor Hubs

There will be two sensor hubs on the pod one located at the front of the pod and one at the rear. Each hub will consist of an Arduino Mega with a CAN shield to allow for communication to the MEB and other shields depending on the sensor type. These hubs will be responsible for receiving data from the sensors and encoding it to allow for transmission on the CAN bus back to the MEBS.

Below is a list of all sensor types on the pod.

Sensor Type	Use
Thermocouple	For reading the temperature of a given component
Encoder	For reading the speed of the encoder wheel to determine pod speed.
IMU	For reading the acceleration of the pod
Distance Sensor	For reading the air gap of the LIM
Voltage	Measure voltage on each phase that is being sent to the LIM
Current	Measure current on each phase that is being sent to the LIM
Frequency	Measure the frequency of power that is inputted into each phase of the LIM.
Barometer	Measure Pressure
Proximity	Determine the deployment of brake pads.

Table 11, Sensor List 1

Below is a list of all sensors on the pod.

Sensor Model ID	Type	Subsystem	Location
DW-AS-511-M30-002	Distance	Stabilizers	Stabilization Arms
ADIS16448BMLZ	IMU	Embedded	Main Control Box
BMP180	Barometer	Power	HV Pressure Vessel
HTTC36-K-116G-6	Thermocouple	LIM	Lim Coils
WTK-6-60	Thermocouple	LIM	Attached to LIM

BAW002C	Distance Sensor	LIM	Attached to the ends of each LIM
INA223	Voltage	LIM	Attached to power input of LIM
MCR-SL-CUC-100-I - 2308027	Current	LIM	Attached to the Power input of LIM
GX-F12B-P	Proximity	Braking	2 sensors for each brake pad
H25 Incremental Optical Encoder	Encoder	Stabilizers	Attached to stabilizer wheels

## 10.4. Control Hub

The control hub is a board connected to the MEB via CAN that receives the control commands sent by the MEB and relays the commands to the individual subsystems. The Control Hub will be connected to the braking, LIM and battery subsystem.

## 10.5. BMS Hub

There are 3 BMSs, one HV BMS and two 24V BMSs. Both the HV BMS and the two 24V BMS will be connected to the MEB via CAN. The MEB will control the HV Battery through commands to the BMS. The two 24V batteries will be directly controlled by the MEB.

## 10.6. Testing

### 10.6.1. Vacuum testing

Vacuum testing will be performed on all parts of the control system that are operating in a reduced pressure environment. The main controls will be placed in the pressure vessel and will not be subject to reduced pressure. This testing will ensure that the control system components will be able to operate without issues in the reduced pressure.

### 10.6.2. Hardware in loop

Hardware in loop testing will be completed on the embedded system using a Raspberry Pi or Arduino to simulate sensor input data and CAN data packets. The reaction of the MEB and the hubs will be recorded and evaluated to ensure that the system is operating as intended.

## 10.7. Single Point of Failure

The Single Point of Failure that is present in the embedded system is the reliance on the CAN bus for main data communication. If the CAN bus loses signal integrity the MEB and the hubs will be unable to communicate. If this happens each hub will go into the mode as outlined in the controls section. This will result in power being cut to the LIM and the breaks being automatically deploying will bring the pod to a safe and controlled stop. After the pod stopped, this is one of the cases where the pod will be unable to crawl back to the end of the track and will need to be manually removed from the track. Although there is a single point of failure in this system we believe with the correct software even with a CAN bus failure the pod still will be able to safely end a run.

## 10.8. Failure Modes

Below is a table of failure modes and the effect on the rest of the pod.

Failure	Description	Result
MEB	Loss of one MEB	Second MEB takes Control Run Aborted
MEB	Loss of both MEB	All hubs lose connection pods enter Failure mode
Control Hub	Loss of Control Hub	Brakes deploy as fail safe MEB shutdown LIM and battery.
Sensor Hub	Loss of Sensor Hub	MEB losses data from Sensor Hub Run Aborted
Sensor	Loss of data input from Sensor	Sensor Hub relays failure to MEB Control system attempts mitigation If mitigation fails Run Aborted
BMS	Loss of BMS	Brakes deploy as fail safe HV battery will be disconnected from system MEB shutdown LIM and battery.

## 10.9. Embedded Bill of Materials

Name of Component	Quantity

Raspberry Pi 3 Model B	2
Pi Can 2	2
ARDUINO MEGA 2560 REV3	3
CAN BUS Shield V2.0	3
8 Channel K-Type EGT CAN Module	1
2 Channel CAN-Bus Thermocouple Interface K-Type	3
250 m Range Time-of-Flight Sensor	1

# 11. Control systems

## 11.1. Overview

The control system of the pod was designed like the embedded system with a focus on redundancy and modularity. The arduino controllers will be programed in the arduino language while the Raspberry Pi controllers and the base station will be programed in Python. If we discover that Python is too slow for this application, we will switch over to C++.

## 11.2. Pod state diagram

The control system for the pod is based on a state machine to ensure that only the correct function can be performed at each state. The control system uses the states provided by SpaceX; the states mirrored the operation of our pod and eliminated the need for mapping.

Pod states:

1. Fault
  - a. Allowed Actions: Braking
  - b. Disallowed Actions: Main battery power, LIM drive
2. Safe to Approach
  - a. Allowed Actions: Braking
  - b. Disallowed Actions: Main battery power, LIM drive
3. Ready to Launch
  - a. Allowed Actions: Main Battery power
  - b. Disallowed Actions: Braking, LIM drive
4. Launching
  - a. Allowed Actions: Main battery power, LIM drive
  - b. Disallowed Actions: Braking
5. Braking
  - a. Allowed Actions: Braking
  - b. Disallowed Actions: Main battery power, LIM drive
6. Crawling
  - a. Allowed Actions: Braking, Main battery power, LIM drive
  - b. Disallowed Actions:

Pod State Diagram

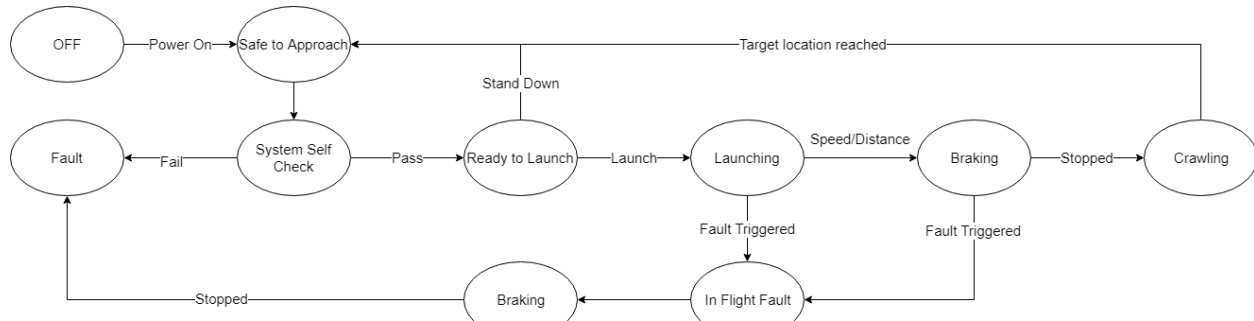


Figure 54, State Diagram

### 11.3. Heartbeat

There will be three heartbeats on the pod: between the two MEBs, between the MEB and Sensor Hubs, and between MEB and control hub. These heartbeats will be used to monitor the operation of the different controllers on the pod and trigger the necessary aborts if needed.

## 11.4. Communication System

Communication between controllers on the pod will be performed via a central CAN bus that will link both main controllers and all sensor and control hubs. The CAN bus was chosen as it is a high speed fault tolerant communication protocol ensuring priority control information is sent.

## 11.5. Navigation System

Pod position will be determined with the encoders on the stabilizer wheels as well as the IMU on board the pod. There will be 2 encoders and the IMU data allowing for 3 data input to allow for error checking. The IMU data with the time elapsed will also allow for speed calculations. We will use a laser distance sensor for crawling phase of the run to ensure that we will stop accurately.

## 11.6. Failure Modes

Failure	Location	Effect
Disconnection	Radio	Pod enters failure state and waits for reconnection
Heartbeat Lost From MEB	Primary MEB	Pod enter failure state and aborts run

Heartbeat Lost From MEB	Backup MEB	Backup MEB takes over control and pod enter failure state.
Heartbeat Lost From Hub	Sensor Hub	Pod enter failure state and aborts run
Heartbeat Lost From Hub	Control Hub	Pod enters failure state and MEB deploy brakes
CAN Bus failure	CAN Bus	Control Hub Stops LIM and deploys brakes. MEB report Fault.

## 12. Next steps

### 12.1. Design Phase

The next phase/step for the uWinloop team involves the following set of tasks:

- 1) Design/Scale SLIM which can operate at desired speed and acceleration.
- 2) Build full scale SLIM which can be tested
- 3) Modify battery based on the power consumption/requirement
- 4) BMS is also needs to be modify based on the changes in the battery
- 5) Pressure vessel needs to be modified/redesign based on the changes of the batteries
- 6) Brake design needs be modified due to increased weight of the vehicle
- 7) Stabilizers needs to modified accordingly
- 8) Frame and shell redesign to accommodate the increased weight, size and change of location of mounting(if so)
- 9) Addition of extra sensors due to changed parameters

### 12.2. Test Phase

Due to air cargo travel schedules, LIM stators will not be available for testing until April 15th at the latest. Until then, all other components will be tested. This includes friction brakes, shell and frame, and battery pack testing.

## 13. Pod Production Schedule

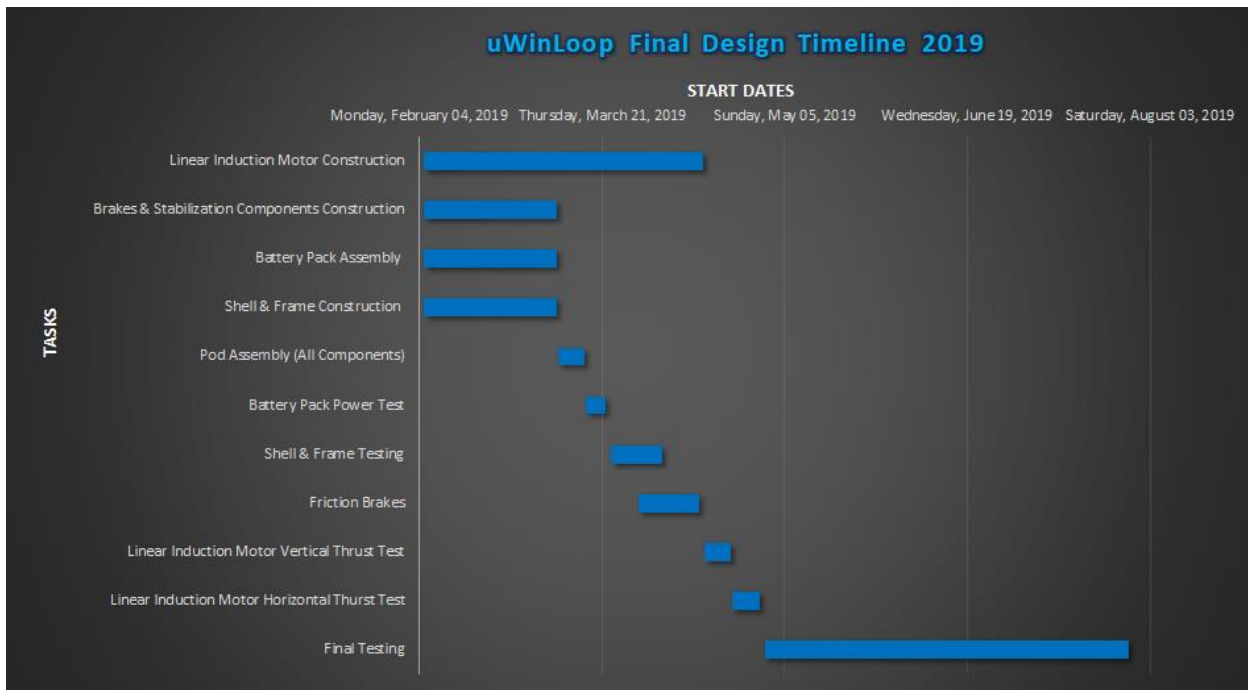


Figure 55, Timeline

## 14. Bill of Materials

MAIN POD COMPONENT	TOTAL PRICE OF COMPONENT
SHELL	5000.00
FRAME	388.64
STABILIZERS	3710.32
BRAKES	5686.68
LIM	1182.32
PRESSURE VESSELS	3414.00
ELECTRICAL COMPONENTS	9194.90
SENSORS	6526.79
EMBEDDED SYSTEMS	4375.10
TOTAL	39478.75

The above chart represents the total price of all major pod components. Total cost breakdown for all materials and each subsequent system of the above pod components is recorded in the final BOM (bill of materials). All prices, although some estimations were necessary, are highly accurate, and have been checked by multiple members of the uWinLoop team for accuracy. Cost estimates (where estimates were necessary), were cross referenced with quotes from various online organizations offering quote services. Averages were taken of the given quotes, leading to the final cost estimates of specific components.

## 15. Financing

If uWinLoop is selected to participate in the 2019 pod competition, multiple individuals and recognizable organizations have agreed to sponsor the construction of the pod. Several of the organizations are familiar with a number of operations at uWinLoop, and are willing to monetarily contribute to the successful design of the pod and its subsystems. Possible sponsors include Ford, FCA (Fiat Chrysler), Siemens, OSPE (Ontario Society of Professional Engineers), Windsor-Essex Economic Development Corporation, Brave Control, FLT (Fibro Laapple Technology Inc.), Advantage Engineering, and Blackberry QNX.

Furthermore, there are several other organizations who will contribute to the creation of the pod by donating materials, manufactured parts, and/or electronics; these other sponsors include: National Instruments, Performance Machinery, Anubis 3D, Windsor-Essex Economic Development Corporation, Kel Com 3D, and Blackberry QNX.

Aside from these main sponsors, if uWinLoop is indeed selected to participate in the 2019 competitions, certain individuals, including a few professors from the University of Windsor, would be ready to monetarily contribute to the construction of the pod. A few professors are currently working with students in preparation for the 2019 competition, to ensure that construction and testing would follow the current guideline set by the team.

## 16. References

LIM Parameters Table

1)

B. Ooi and D. C. White, "Traction and Normal Forces in the Linear Induction Motor," in *IEEE Transactions on Power Apparatus and Systems*, vol. PAS-89, no. 4, pp. 638-645, April 1970.  
URL: <http://ieeexplore.ieee.org/stamp/stamp.jsp?tp=&arnumber=4074110&isnumber=4074092>

2)

Ee. "Basics of Wire Gauge and AWG System." *Basics of Electrical Engineering*, 25 July 2017, [www.basicsofelectricalengineering.com/2017/07/basics-of-wire-gauge-and-awg-system.html](http://www.basicsofelectricalengineering.com/2017/07/basics-of-wire-gauge-and-awg-system.html).